Loess and floods: late Pleistocene fine-grained valley-fill deposits in the Flinders Ranges, South Australia

(excerpt from Hans Heysen 1929: "Foothill of the Flinders", Morgan Thomas Bequest Fund 1939)

David Haberlah

Geology and Geophysics
School of Earth and Environmental Sciences
The University of Adelaide

This thesis is submitted in fulfilment of the
requirements for the degree of Doctor of Philosophy
in the Faculty of Science, University of Adelaide

August 2009

2. Methods

'There is one thing even more vital to science than intelligent methods; and that is, the sincere desire to find out the truth, whatever it may be.' – Charles Pierce

The methods and techniques selected to establish the depositional environment of the Flinders Silts can be grouped into chronostratigraphic, geochemical and geophysical approaches.

The regional chronostratigraphic approach aimed at comparing and correlating aggradational sequences from different geomorphologic settings and catchments. While "marker bands" such as palaeosols were used along single section faces, numerical dating proved to be fundamental to the comparison of sections typically spaced several kilometres apart from each other. It also provided the only means by which to establish the timing and rates of deposition, and the duration of erosional intervals. Previous work (Williams 1982) suggested that the limit of radiocarbon dating could locally be exceeded. Site-specific unavailability of organic material, as well as a recent study questioning the validity of radiocarbon ages from the Homeb Silts in Namibia (Bourke et al. 2003) prompted the design of a regional dating campaign involving both optically stimulated luminescence (OSL) dating and accelerator mass spectrometer (AMS) radiocarbon dating. Standard laboratory methods and protocols were employed, but additional comparisons between radiocarbon ages obtained from different organic material were made. Similarly, small aliquots and single-grains for luminescence dating were juxtaposed, and the results from multiple age models were compared and critically discussed. Luminescence dating was carried out in collaboration with Ed Rhodes at the Australian National University (ANU) luminescence dating laboratory, and Tim Pietsch at the CSIRO luminescence dating laboratory in Canberra. All samples were prepared at the luminescence dating laboratory of the University of Adelaide under the kind supervision of John Prescott and Frances Williams. The same is true for all determinations of all environmental dose rates, equivalent dose estimates, and the final OSL age calculations. Radiocarbon dating involved two weeks of training in sample pre-treatment and combustion at the ANSTO research facilities (Lucas Heights). Additional radiocarbon samples were sent to the ANU Radiocarbon Laboratory and the Waikato Dating Laboratory.

The largely homogenous, fine-grained and partially-aggregated material required an integrated high-resolution sediment-sizing and advanced statistical particle-size distribution analysing approach, developed over repeated visits to the sedimentological laboratory of Griffith University (Brisbane)

under the kind supervision of Grant McTainsh. The results are presented in form of a paper in section 2.3.

Finally, a range of well-established and emerging analytical techniques was applied to determine the local vegetation, hydrological and weathering history of the layered to laminated section BRA-SD ('Slippery Dip'). This involved quantitative mineral spectroscopy, induced magnetic susceptibility measurements and isotopic carbon geochemistry, the methods of which are summarised with the results as a manuscript in section 3.2.

Over the course of this study, the importance of careful field observations and detailed lithofacies mapping was realised and given appropriate time. The main results are summarised together with the chronostratigraphies in relevant papers in sections 3.1 and 3.2 and the corresponding appendices.

2.1 Optically Stimulated Luminescence dating

'The sand so pale it might be grains of light' . – Roselle Angwin

Optically Stimulated Luminescence (OSL) dating is a relatively new method in the field of radiometric dating (Huntley et al. 1985). Its underlying principle is based on the characteristic of common mineral grains such as quartz sand to accumulate stored energy in their crystal lattices which is released on exposure to light. Consequently, sediments buried by a depositional event gradually acquire an increasing charge which can be freed and measured in the laboratory by stimulation with a beam of light. From this, the time elapsed since burial, i.e. the age of the sedimentary unit, can be resolved by establishing the environment-specific average energy flux the constituent sample grains were exposed to.

OSL dating is closely related to Thermoluminescence (TL) dating and Electron Spin Resonance (ESR) dating, where stimulation by heat or electromagnetic field is used to depopulate electron traps in mineral grains (Aitken 1985). The great advantage of OSL over TL and ESR for palaeo-environmental studies is based on the prevalent and comparably rapid mode for re-setting the radiometric clock or "luminescence signal" of mineral grains in nature: the exposure to daylight during erosion, transport and deposition. Optical stimulation only samples "light-sensitive" electrons at a trap depth freed by light (Huntley et al. 1985). Electrons ejected from such traps within the crystal lattice recombine and release energy, some in the form of luminescence. With the help of a photomultiplier, these photons are converted to electric pulses and measured (Aitken 1998). Since, single quartz grains, or aliquots of such, behave differently to irradiation, it is important to individually assess that sensitivity. This is done by comparing the natural luminescence signal to responses to a sequence of laboratory radiation doses (Murray & Wintle 2000). The dose required to produce a luminescence signal equal to the measured natural signal is called equivalent-dose (D_e), measured in grays (Gy = 1J/kg), and is the numerator of the OSL-age equation [1]. The denominator consists of the average rate of energy flux absorbed by the sample in its natural depositional environment. This is referred to as dose-rate (DR), and expressed as grays per kiloyear (Gy ka^{-1}):

[1] $OSL\text{-}age\ (ka) = D_e\ (Gy) / DR\ (Gy\ ka^{-1})$

The DR absorbed by the sample mineral depends on its exposure to radioactivity from the decay processes of naturally-occurring radioactive elements within the sediment and on cosmic irradiation. These produce secondary electrons through ionisation in the crystal lattice which subsequently

become trapped in structural defects. Energy absorption increases proportionally over time until all available traps are filled and the mineral becomes "saturated" (Aitken 1998). Hence, the upper limit of the OSL dating range is a function of the natural radioactivity of a given sedimentary unit, the mineralogy of its constituent grains and the burial time. Dose response curves of quartz grains generally become non-linear at ~30 Gy and saturate before ~150 Gy (Prescott & Robertson 1997), often limiting the OSL dating to the last glacial cycle (Walker 2005).

The accuracy of the OSL-age determination of a depositional event is impaired by the following factors affecting D_e and DR, respectively. The largest potential source of error affecting the D_e arises when the depositional context prevents an effective re-setting of the luminescence signal, resulting in so-called "partial bleaching". While OSL dating encounters significantly less residual signals than TL dating, for light-sensitive traps of quartz grains the signals are reduced to a negligible level in only a few seconds of exposure to daylight (Murray & Olley 2002), this prerequisite is not always achieved in all transport media, durations, compositions and saturations, or at night time (Bourke et al. 2003). Variation in the resultant luminescence signal is dealt with by establishing the spread of D_e-values over multiple individual grains or small aliquots for a given sample, and by applying appropriate protocols and age models in the interpretation of the D_e frequency distribution (Olley et al. 1998; Murray & Wintle 2000; Duller 2004; Jacobs et al. 2006). The DR on the other hand is affected by variations in the water content over the burial time of the sedimentary unit, pedogenic alterations of its mineral composition, and changes in the thickness of the overburden; all of which require a site-specific model for corrections. Further, mobile nuclides in the uranium decay chain can result in both loss and augmentation of radionuclides and consequent changes in the rate of delivery of the radiation dose. Radioactive disequilibrium can be assessed by comparison of results for the uranium (and thorium) decay chain members obtained by different methods (Prescott & Hutton 1995).

Finally, sources of systematic errors arise from the employed techniques, precision and calibration of instruments and data conversions, limiting the precision of OSL-age determination (Murray & Olley 2002; Jacobs et al. 2006).

Field sampling

These sources of errors need to be kept in mind while deciding on stratigraphic sections and sedimentary units to sample for OSL dating. In terms of DR evaluation, this translates to strata where post-depositional disturbances such as diagenetic pedogenic alterations, fluctuating water tables (leaching) and more general variations in the water content can be assumed minimal over the time of burial. Since gamma rays contribute from as far as 30 cm to the ionising radiation, OSL samples

should ideally be surrounded by the same (homogenous) strata and lie below the surface by this distance (Aitken 1998). In terms of D_e evaluation, bioturbated strata prone to contamination with younger material must be avoided. The depositional modes that form a given stratigraphic sequence should be assessed for resetting the radiometric clock. While aeolian accessions such as loess mantles have the best "bleaching" potential, this is less so for a variety of fluvial deposits. Colluvial sediments such as slope wash can prove very difficult to date, potentially reflecting multiple partially-bleached cycles of erosion and deposition resulting in large apparent OSL-age variations (Prescott & Robertson 1997).

Finally, the employed sampling procedure must shield the sample from present-day light. For this study, all samples are extracted from the selected strata by hammering steel cylinders of 12.5 cm length and 6 cm diameter into vertical sections, after scraping them clean and level. A ball of aluminium foil is inserted into the cylinder first, reducing shake-up of the sediment sample in the cylinder during extraction and flattening out to an opaque seal towards the end. Both ends are sealed by black plastic lids and the sample is placed in an air-tight sample bag to minimise changes in the present-day water content for subsequent measurement in the laboratory. Wherever feasible, OSL samples are paired or bracketed by radiocarbon samples.

Environmental dose-rate estimation

The luminescence signal is proportional to the amount of ionisation which in turn is proportional to the energy absorbed from radiation from the sample environment. An accurate measurement of the environmental dose-rate (DR) and a critical assessment of possible changes over the time of burial determine half the age equation. Methods of DR determination and conversion factors are well-established (Aitken 1985; 1998; Adamiec & Aitken 1998) and have remained much the same over the past decade (Duller 2004). For most OSL samples, the DR is produced in roughly equal proportions by the decay of the naturally-occurring radioactive isotopes potassium-40, and the decay chains of the radionuclides of Thorium-232 and Uranium-238. The range of ionising and highly saturating alpha particles is <5 µm, and is effectively removed during sample preparation. Beta radiation, i.e. electrons, penetrates a few millimetres, and the gamma radiation up to a distance of 30 cm through sediments (Aitken 1985). Hence, DR determination requires a detailed analysis of the radioactive elements in both the sample and its surroundings.

In addition, a usually small but not negligible DR contribution is derived from cosmic rays. The exact amount varies with altitude, latitude and sample depth, as well as with long-term time variations in galactic primary cosmic ray intensity and near earth modulation by changes in solar conditions and the geomagnetic dipole moment (Prescott & Hutton 1994). For the geomagnetic latitude (~31°), age

range (LGM) and altitude (<400 m) for the presented samples, shielding afforded by the overburden (e.g. ranging from 35 to 1465 cm for WL07-FP) is deemed significant and calculated employing formula [2] published in Prescott & Hutton (1994) (see appendix 5.2.1.1).

In order to test for radioactive disequilibrium in the potentially problematic (wet) alluvial depositional environment of sampled stratigraphic sections, laboratory measurements of the radioactive elements by combined X-ray fluorescence spectrometry (XRS) for potassium-40 (K) and "Thick Source" Alpha Counting (TSAC) for thorium (Th) and uranium (U) are conducted for all samples and compared to independently obtained data from reactor-based Delayed Neutron Analysis (DNA) and *in-situ* field scintillometry (Hutton & Prescott 1992). No disequilibrium was established in terms of statistically significant discrepancies between results for radioactivity of the U and Th decay chain members between differing methods (Prescott & Hutton 1995).

Dose-rates based on all measurements discussed below are calculated using the DOS-based "AGE99" software (Grün 1994). For *in-situ* derived K-, U-, and Th-contents and the total gamma ray count, adjustment for water content is required, using the following equation (Aitken 1985):

$X_{(dry)} = X_{(moist)} * (1 + F * H_2O\text{-content})$

F = 1.14 for total gamma count, 1.10 for K and U, 1.09 for

For the computation, information regarding the diameter of the grain-size fraction used for the D_e estimation, the thickness of the outer layer removed during sample preparations, the average water content, and the cosmic ray estimate are required. The detailed protocol is given in appendix 5.2.1.2.

Scintillometer field measurements

The most advantageous method of evaluating the environmental DR for a given sample is by using a field gamma spectrometer for *in-situ* measurements of the radioactivity of the three main emitters. The measurement time (~30 min) is fast compared to the work load involving alternative and complementary laboratory measurements and calculations described below. Further, *in-situ* measurements best take account of the natural heterogeneity of the sample environment. However, since the detecting crystal needs to be inserted at least 30 cm clear of all surfaces (Aitken 1985), the extraction hole needs to be deepened and widened. Thereby, a source of uncertainty is introduced by departing from the actual and immediate sample-specific irradiation environment. The measurements for the individual radioactive components assume equilibrium in the U and Th decay chains (Prescott & Hutton 1995).

Scintillometry is based on the characteristic of gamma photons to produce scintillation pulses in sodium iodide crystals corresponding to their full energy of emission. These are converted to individual spectral "photopeaks" by a photomultiplier. Potassium-40 and the Th and U decay chains emit photons of characteristic energies resulting in a composite of such photopeaks. (Aitken 1985). Within this continuum, the following photopeaks best relate to the main DR components; 1.46 MeV for potassium-40, 1.76 MeV for bismuth-214 of the U-series (with correction for interferences) and 2.62 MeV for lead-208, the last member of the Th-series (Prescott & Hutton 1995).

In collaboration with J.R. Prescott and F. Williams, the Adelaide portable multichannel gamma ray spectrometer (EXPLORANIUM) housing a 76 x 76 mm area low background sodium iodide scintillation crystal was employed at some sample locations. In addition to the spectral windows for the three radionuclides, the total gamma ray activity (0.5 – 2.78 MeV) was recorded (Prescott & Hutton 1987). The large size of the crystal requires no correction for the rate of muons from the cosmic ray flux, with the largest contribution to the measured count located in the Th spectral window (2.46 – 2.77 MeV) below ~0.7 %, well within the instrumental counting uncertainty of 2.2 % (Prescott & Clay 2000). The spectrometer is introduced horizontally into the sample holes which are widened to 80 mm diameter and deepened to 60 cm.

All on-site spectrometry values (converted to their dry equivalent) are reported in appendix 5.2.1.

"Thick Source" Alpha Counting and X-Ray Fluorescence spectroscopy

Alpha counting in combination with an alternative method to determine the contribution of non-alpha particle emitting potassium-40 is the preferred laboratory technique of DR estimation. The applied technique of "Thick Source" Alpha Counting (TSAC) has the advantage of being simple, inexpensive and reliable. The sample to background ratio is high and by employing the so-called "pairs technique", U- and Th-contents can be discriminated (Aitken 1985). Disadvantages are long counting times that together with background and statistically viable "pairs" measurements can take up to a week, followed by arithmetic work load.

TSAC is based on the principle that alpha particles emitted by a representative dry and powdered sediment sample placed in close contact with a zinc sulphide scintillation screen cause scintillations of light. Amplified by a photomultiplier and converted to sizeable electrical pulses, the alpha activity of the sample is counted. Zinc sulphide is largely insensitive to beta and gamma radiation, resulting only in minor signals that are rejected by a discriminator unit (Aitken 1985). The combined U- and Th-alpha activity can be discriminated by the "pairs technique" making use of the fact that ~3 % of counts related to the Th decay chain occur as near pairs (within 0.14 ms of each other) as the result

of the very short half life of alpha emitter polonium-216. “Pairs” are separately counted and with the help of an electronic coincidence circuit used to infer separate U- and Th-contents.

An inexpensive laboratory method to measure the K-content is by X-Ray Fluorescence spectrometry (XRF). It is based on characteristic "secondary" (or fluorescent) X-rays produced by primary X-rays striking a thick and very homogenous sample (Hutton & Prescott 1992). The XRF machine used at the Mawson Laboratories of the University of Adelaide determines potassium-40 contents with a precision of >97 %.

Detailed protocols for both TSAC and XRF analyses are given in appendices 5.2.1.3 and 5.2.1.4. The final conversion results based on Adamiec and Aitken (1998) are listed in appendices 5.2.1.5 and 5.2.1.6.

Effect of water content variations

Water attenuates ionising radiation more strongly than constituent mineral grains of the sedimentary unit and introduces the largest uncertainty in the calculation of accurate DR estimates (Aitken 1998). While present-day water contents can readily be measured in the laboratory and adequately taken into account in the final DR calculation, they do not necessarily represent the average water content within the sediment over its time of burial (Li et al. 2008). A simple test, using constrained K-, U-, and Th-values and a specific D_e estimate, was conducted with the “AGE99” software (Grün 1994). The result emphasises the sensitivity of the DR and thereby OSL estimate to such variation (see Fig. 2.1A). Accordingly, an increase in the water content from zero to 10 % results in an increase of the apparent OSL-age by 6.9 %.

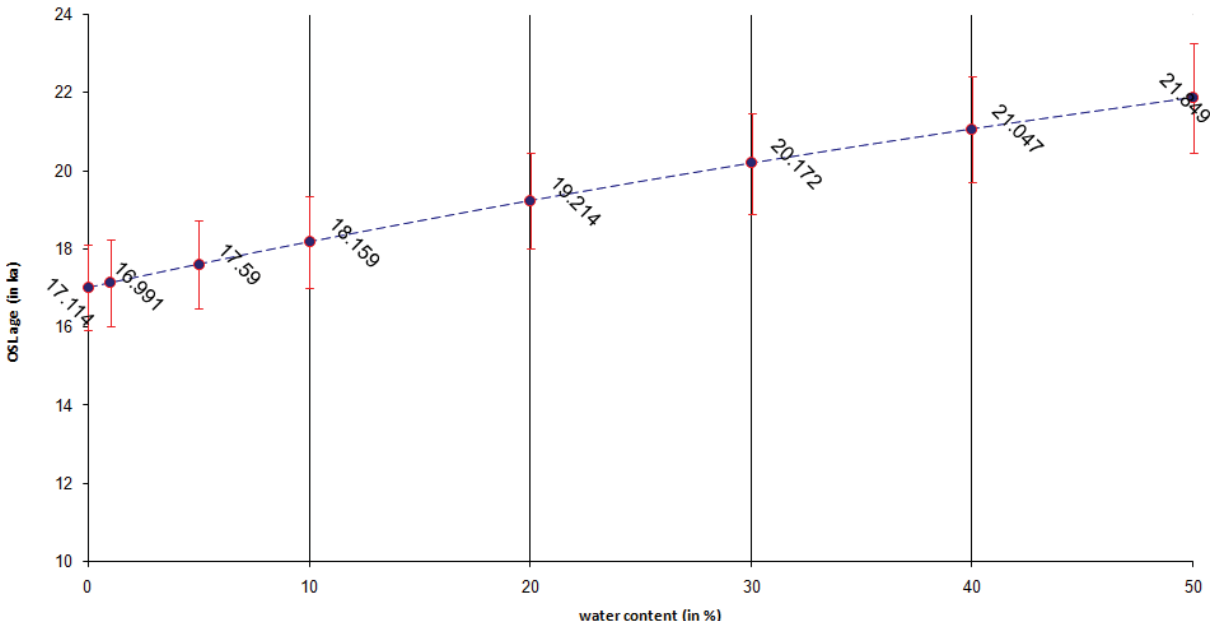

Fig. 2.1A) *The isolated effect of water content variations on the apparent OSL-age for sample WL07-FP6 (SA).*

Equivalent-Dose Estimation

The intensity of the luminescence signal increases with the radiation dose in a nonlinear way differing for every sub-sample of quartz grains. In order to translate the measured natural luminescence signal into an accurate laboratory equivalent-dose (D_e), the aliquot-specific response to a sequence of administered radiation doses is established. Complications arise from sensitivity changes and partial transfer of deeply trapped charges within the mineral lattice over the sequential process of irradiation and resetting.

Single-Aliquot Regenerative-Dose Protocol

A recent analytical breakthrough in OSL dating was achieved by development of a method that accounts for both intrinsic variations in the luminescence intensity between grains and the sensitivity changes that occur throughout the dating procedure (Murray & Wintle 2000). The fundamental idea of the single-aliquot regenerative-dose protocol (SAR) is to compare the initially measured natural OSL signal with equivalent sensitivity-corrected signals from laboratory-administered irradiation-dose responses performed on the same aliquot. Doses are incrementally increased beyond the value of the natural signal resulting in a dose-response “growth curve”. The D_e-value for a single aliquot is obtained by projecting the natural sensitivity-corrected OSL signal onto the growth curve and identifying the point of interception. Changes in luminescence that result through thermally resetting the luminescence signal between measurements, i.e. eliminating all

residual trapped charges, are monitored by interposing fixed test doses. The measured response is used to normalise the sequence (Murray & Olley 2002).

The SAR protocol is employed for all the present samples and the data are processed with the scientific software Analyst 3.22b™ (Duller 2005). One fundamental advantage of the SAR protocol over previous methods is that it allows for internal checks to exclude deficient aliquots based on their recycling ratio, test dose errors, background difference and curve-fit (Wintle & Murray 2006). Only a small number of quartz grains result in acceptable growth curves that can be used to infer reliable D_e-values. Tests checking the integrity of aliquots performed on the presented data are based on the rejection criteria recommended by Jacobs et al. (2006). The most important are the sensitivity correction-recycling ratio test performed by repeating the first measurement at the end of the sequence of progressive and corrected sensitivity changes, here set not to exceed >10 %, and the signal intensity test set to demand a minimum intrinsic brightness of valid aliquots of more than three times the background.

Aliquot Selection and D_e Calculation

Variations between D_e-values of multiple aliquots for any given sample result from insufficient exposure to daylight, variable exposure to the flux of ionising radiation within the sedimentary unit, and contamination with more recently bleached material. Only in exceptional geomorphic circumstances are all grains sufficiently exposed to reset their pre-existing luminescence signals. Particularly in fluvial and colluvial environments, a potentially large fraction retain prior D_e-values. Including such poorly-bleached aliquots in the final D_e calculation for the sample will result in a potentially significant OSL-age overestimation (Olley et al. 1998). It follows that it is crucial to establish the variability in distribution of D_e estimates and, by making assumptions on the cause of the observed heterogeneity, determine the one representative of the depositional event to be dated.

Variability of D_e-values from a sample is best addressed by reducing the aliquot size, thereby minimising the effect of averaging. With the development of luminescence readers designed for rapid single grain measurements (Duller et al. 1999), this can now be achieved on the basis of single grains. However, since only a small number of quartz grains produce a valid signal (Duller 2004), similar results are achieved by reducing the aliquot size to the smallest “effective” number of grains. This is demonstrated by OSL sample WL07-FP 6, for which the D_e was independently established by single grains and small aliquots of ~20 grains (see Fig. 2.1B). It is now common practice to run at least 12 replicate measurements on small aliquots to assess the error on the overall D_e estimate (Duller 2004).

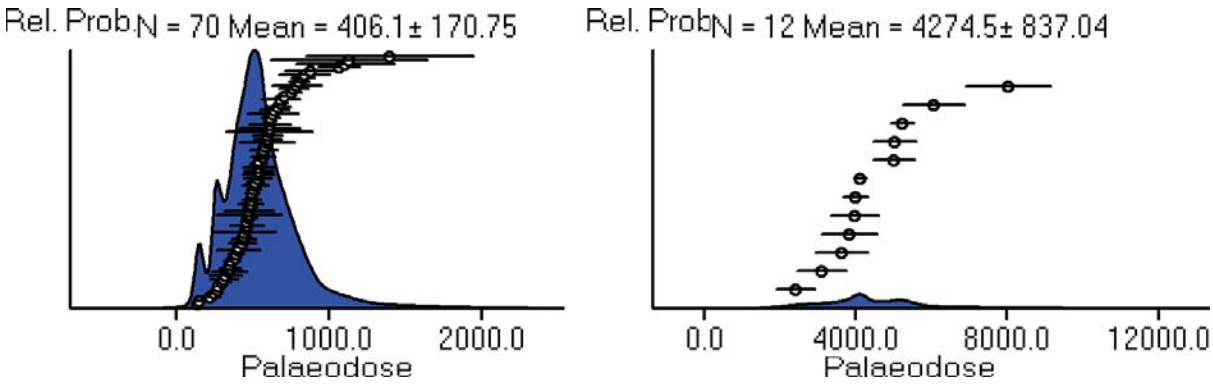

Fig. 2.1B) *Comparison of the variability in D_e-values between single grains and small aliquots (~20 grains) for sample WL07-FP 6 in the form of probability density plots using Analyst 3.22b™. Note that calibrated overall D_e estimates are near identical when converted to Gy (56.44 ± 6.19 Gy vs. 57.38 ± 3.51 Gy).*

Sample D_e estimates based on averaging D_e-values across all reliable aliquots can result in OSL-ages with little relevance to the actual depositional event. Tails of large D_e-values in frequency distributions reflect partially-bleached aliquots (see Fig. 2.1B). Depending on the sedimentological context, a fraction of exceptionally small D_e-values can further reflect post-depositional processes, i.e. bleached grains subsequently introduced by pedogenic activity such as infiltration, desiccation cracking and bioturbation. It is therefore essential to establish discrete populations of D_e-values and limit the D_e calculation to fully-bleached aliquots representative of the depositional event to be dated. With prior knowledge of the sedimentological context of the sample, misleading D_e-values can be manually excluded by graphically- and statistically-aided classification estimates based on probability density and radial plots.

Probability density plots replace the D_e-value of each aliquot with a Gaussian density function with a standard deviation equal to the error of the D_e estimate. All D_e-values are summed point-wise to produce a continuous frequency distribution curve. D_e-values with respective error bars can be added as interval plots, so that the number and spread of components forming modes can be assessed (see Figs. 2.1B & C). While probability density plots are visually intuitive and produce an overall error for selected D_e-values, they are problematic in that they confound D_e variation with error estimation, or as (Galbraith 1998) points out, "... obscure[ing] good information in the data by inappropriately weighting in with poor information". More importantly, weighted histograms offer no sound statistical basis to the interpreter to decide upon which group a given aliquot belongs to.

Radial plots on the other hand display variability in D_e-values for a sample by plotting aliquots as points with their precision against the abscissa and their D_e-value against the ordinate. The latter is

scaled in terms of standard deviations from a given central value or "radial line" (see Fig. 2.1C). More precise D_e-values plot towards the right and statistically concordant ages fall within a band of two standard deviations about the radial line (Galbraith 1990). Different radial lines correspond to different central D_e-values. Populations, where more than 5 % of the constituent aliquots fall outside the two standard deviations band, are termed "over dispersed". Ideally, the interpretive classification estimate results in a single discrete population of D_e-value with a Gaussian distribution. Multiple populations, representing a more complex geomorphic history and the occasional younger and older outliers stand out clearly (see Fig. 2.1C).

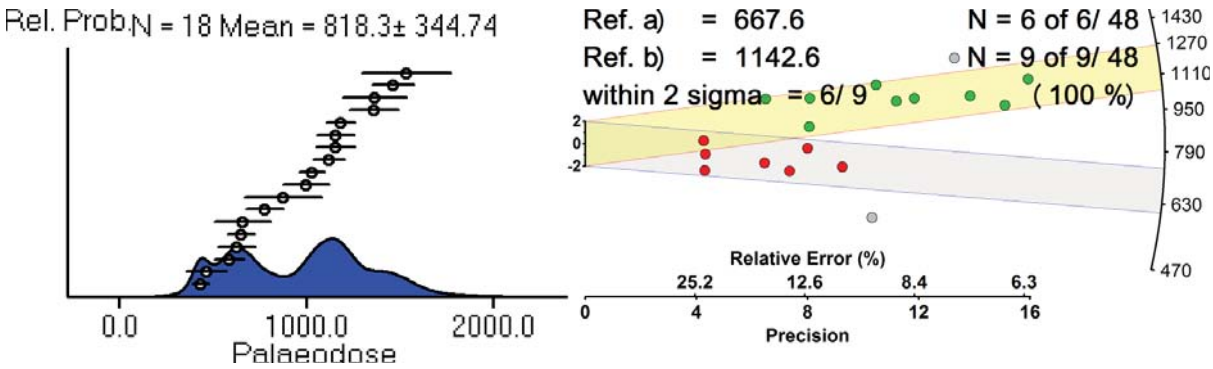

Fig. 2.1C) *Comparison between the probability density plot comprising all reliable aliquots and the corresponding radial plot for sample WL07-G 1. D_e-values fall either within one of two discrete near-Gaussian populations around a "younger" (red) and an "older" (green) radial line, or are rejected as outliers.*

The interim and final results of the D_e-value selection and corresponding age estimates are presented as probability density and radial plots in appendix 5.2.1.7.

Equivalent-Dose Sample Preparation

All samples are prepared for D_e estimation following the protocol of the University of Adelaide luminescence laboratory (see appendix 5.2.1.8). Physical and chemical pre-treatments are conducted with the aim of isolating a homogenous fraction of clean quartz grains for small aliquot (~20 grains) and single grain measurements. The partially-aggregated nature of the sample material requires thorough disintegration by ultrasonic bath and alkali washes (NaOH). Carbonates and organic matter are removed in 20 % HCl and 30 % H_2O_2, respectively. Treatment with 40 % HF dissolves feldspars and etches the outer rind of the quartz grains affected by alpha radiation. Heavy liquid separation employing Lithium Polytungstate with a specific gravity 2.67 g/cm^3 and magnetic separation are used to remove heavier minerals and quartz grains with ferrous coatings or

inclusions. Owing to the very fine nature of the sediments, the chemical treatment was conducted on two separate size fractions; the preferred 180-212 µm aliquot, and the finer 125-180 µm aliquot as a fallback option. In order to remove potential broken quartz grains and only partially dissolved feldspars, both size fractions are re-sieved using 150 µm and 90 µm sieves, respectively.

Final sample quantities are generally less than 0.5 g for the larger (>150 µm) fraction, and in two instances the more abundant finer fraction (>90 µm) fraction had to be used (appendix 5.2.1). A few samples did not yield sufficient grains altogether and had to be re-sampled or substituted by alternative samples.

OSL data discussion

According to single grain studies performed on samples from the Wilkawillina Silts, on average only one in ten grains of quartz records a valid photon count. This value varies from 4 to 16 % among samples. Partial bleaching is the norm and addressed by minimising the aliquot size to an "effective" number of ~20 grains where no single grain analyses could be performed. Independent results for single grain and small aliquot analyses are obtained for methodological comparison for sample WL07-FP 6. While the spread in D_e-values is most pronounced and therefore best recorded by single grains, the weighted overall D_e estimates turn out statistically identical (see Fig. 2.1B).

Wherever feasible, OSL-ages are paired with or bracketed by calibrated AMS-ages. It is important to keep in mind that thereby dated events, i.e. concealment of quartz grains from daylight and the last uptake of carbon from the atmosphere by embedded organic material, are not necessarily synchronous (see section 2.2).

A twofold approach was applied to obtain OSL-ages with a meaningful measure of uncertainty. Firstly, separate DR estimates are calculated for all independent laboratory and field measurements. These are corrected for a range of potential water contents over the burial time of the sedimentary unit, since this variable constitutes the largest source of uncertainty on part of the DR estimation. Measured present-day water contents range from ~2.5 to ~10 % across all samples and, where re-sampled, are found to vary ~5 % between seasons. Hence, these values are used to calculate a maximum and a minimum DR estimate for each sample. In addition, a "most likely" estimate is determined by averaging the DR estimate for the somewhat arbitrary measured present-day water content with the median DR estimate for a "balancing" 5 % water content (see Fig. 2.1D and appendix 5.2.1).

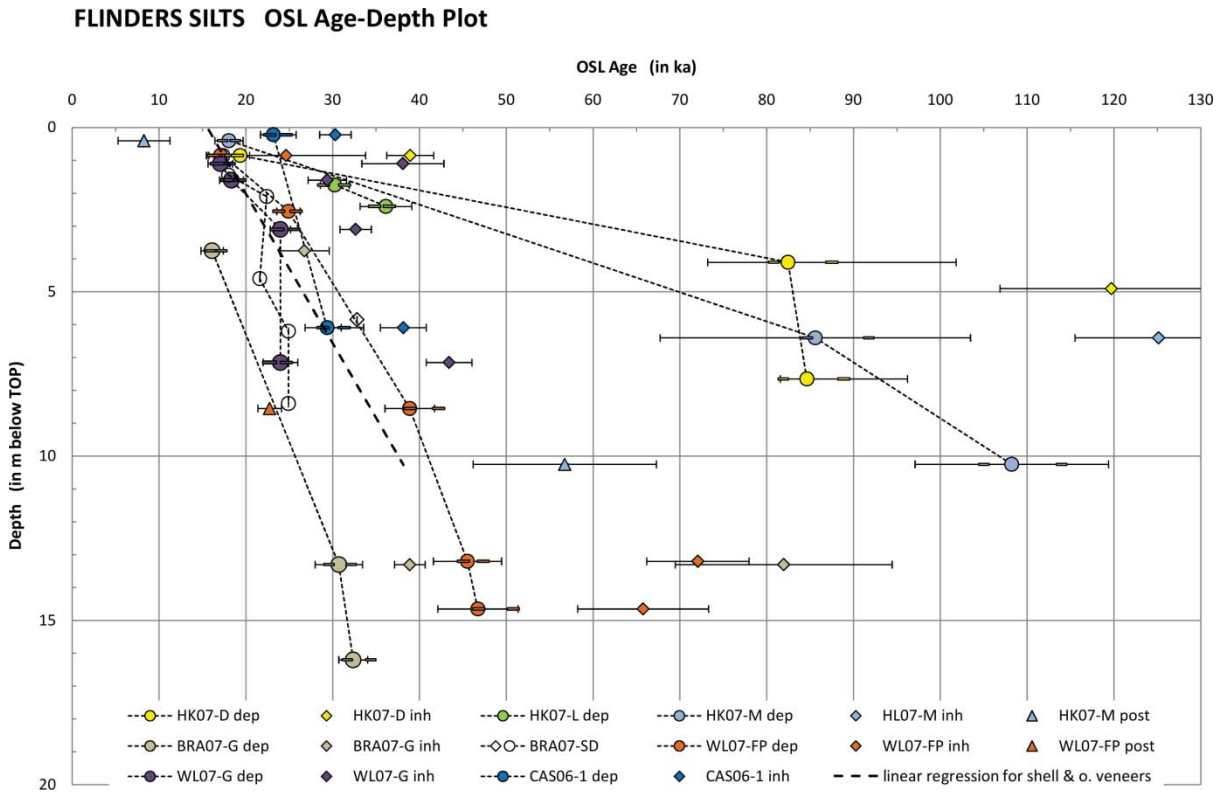

Fig. 2.1D) *Flinders Silts optically-stimulated luminescence (OSL) data, colour-coded by stratigraphic section. Age estimates referring to the last depositional event are depicted as circles, flanked by rectangles indicating the impact of changes in water content for 2.5 % and 10 %. Significant "inherited" D_e-populations are plotted as diamonds and significant "post-depositional" De-populations as triangles. The linear regression for AMS-dated shells is indicated for comparison with Fig. 2.2D).*

Secondly, D_e estimates are calculated by the following three-fold approach. Sets of all reliable aliquots based on the rejection criteria suggested by Jacobs et al. (2006) are compiled from best curve-fits using Analyst 3.22b™ (Duller 2005). These are independently analysed by the two statistical OSL-age models most commonly applied to partially-bleached sediments; the Minimum Age Model (Olley et al. 1998) and Finite Mixture Model (Galbraith 1988; Galbraith & Green 1990). The appropriate application of statistical age models in determining the population of D_e-values most likely to represent the last depositional event depends on the sedimentological context and can vary throughout the aggradational sequence. The Minimum Age Model (MAM) can be problematic in the context of post-depositional disturbances (Jacobs et al. 2006). The Finite Mixture Model (FMM) generates multiple populations of aliquots with similar apparent ages, requiring an interpretation within the stratigraphic context.

In an alternative procedure, the OSL data are first analysed by an iterative manual approach determining discrete D_e populations to which the Common Age Model (Galbraith et al. 1999) is applied. Accordingly, sets of all reliable aliquots are displayed as probability density plots and radial plots as automatically generated in Analyst 3.22b™, providing a general idea of the spread of aliquots and number of modes. By applying the Common Age Model (CAM), i.e. the weighted mean across all reliable D_e-values, an initial estimate is calculated and recorded (see appendices 5.2.1 and 5.2.1.7). Consequently, discrete populations are discriminated. While cumulative weighted histograms are not an appropriate means by which to establish discrete populations *per se* (Galbraith 1998) they can assist in laying out the radial plots. Apparent modes of aliquots are entered as central values for radial lines in Radial Plot 1.3™ (Olley & Reed 2003) to see if they encompass the inferred populations and, if so, establish which of the aliquots fall within two standard deviations. Subsequently, outliers are excluded from the probability density plots and the central age of the subsets is determined. The results are entered as central values in the radial plot. The process is repeated if new aliquots are encompassed by the shift of the two standard deviations wide band around the radial line. Finally, aliquots with large errors and little effect on the overall D_e estimate are excluded from the final calculations in order to reduce the OSL-age uncertainty. This step is followed by last adjustments of radial lines according to the final weighted means of the D_e-value populations. The aliquots within the radial plots are colour-coded for documentation purpose; those within two standard deviations and part of the final D_e estimation in red, those falling outside but still part of the final D_e estimation in blue, and all aliquots rejected on account of being significant outliers or contributing only noise are depicted in grey. Some samples were found to encompass two significant discrete populations of D_e-values; a “younger” displayed in red and an “older” in green (see Fig. 2.1C). Averaging across such populations would result in an overall D_e estimate that would translate into an erroneous OSL-age, i.e. an age estimate with no significance to any single bleaching process. Where two populations are encountered, the “younger” is interpreted to represent the last transport/depositional event or significant post-depositional disturbance. Consequently, the “older” is interpreted to represent a previous bleaching event unaffected, or only partially affected by later transport process(es) and therefore possibly relating to the age of the sediment load prior to its re-deposition. Both overall D_e estimates are recorded (see 5.2.1 and 5.2.1.7).

The manual approach is further complemented by the Finite Mixture Model (Galbraith 1988; Galbraith & Green 1990) applied to obtain D_e estimations for all OSL samples. The protocol is discussed together with the results in the manuscript of section 3.1. Full documentation is given in appendices 5.2.1 and 5.2.1.9.

References

Adamiec, G., Aitken, M.J. 1998. Dose-rate conversion factors: an update. *Ancient TL* **16(2)**, 37-50.

Aitken, M.J. 1985. *Thermoluminescence Dating*. Oxford, Academic Press.

Aitken, M.J. 1998. *An Introduction to Optical Dating*. Oxford, University Press.

Bourke, M.C., Child, A., Stokes, S. 2003. Optical age estimates for hyper-arid fluvial deposits at Homeb, Namibia. *Quaternary Science Reviews* **22**, 1099-1103.

Duller, G.A.T. 2004. Luminescence dating of Quaternary sediments: recent advances. *Journal of Quaternary Science* **19(2)**, 183-192.

Duller, G.A.T. 2005. *Analyst 3.22b*. Aberystwyth, United Kingdom, Institute of Geography and Earth Sciences, University of Wales.

Duller, G.A.T., Botter-Jensen, L., Murray, A.S., Truscott, A.J. 1999. Single grain laser luminescence (SGLL) measurements using a novel automated reader. *Nuclear Instruments and Methods in Physics Research* **155(4)**, 506-514.

Galbraith, R.F. 1988. Graphical display of estimates having differing standard errors. *Technometrics* **30**, 271-281.

Galbraith, R.F. 1990. The radial plot: graphical assessment of spread in ages. *Nuclear Tracks and Radiation Measurements* **17(3)**, 207-214.

Galbraith, R.F. 1998. The trouble with "probability density" plots of fission track ages. *Radiation Measurements* **29(2)**, 125-131.

Galbraith, R.F., Green, P.F. 1990. Estimating the component ages in a finite mixture. *Nuclear Tracks and Radiation Measurements* **17(3)**, 197-206.

Galbraith, R.F., Roberts, R.G., Laslett, G.M., Yoshida, H., Olley, J.M. 1999. Optical dating and multiple grains of quartz from Jinmium rock shelter, northern Australia: part 1, experimental design and statistical models. *Archaeometry* **41(2)**, 339-364.

Grün, R. 1994. *Age99*, version 09/11/1994, Risoe Laboratories.

Huntley, D.J., Godfrey-Smith, D.I., Thewalt, M.L.W. 1985. Optical dating of sediments. *Nature* **313**, 105-107.

Hutton, J.T., Prescott, J.R. 1992. Field and laboratory measurements of low-level thorium, uranium and potassium. *Nuclear Tracks and Radiation Measurements* **20(2)**, 367-370.

Jacobs, Z., Duller, G.A.T., Wintle, A.G. 2006. Interpretation of single grain D_e distributions and calculation of D_e. *Radiation Measurements* **41**, 264-277.

Li, B., Li, S., Wintle, A.G. 2008. Overcoming environmental dose rate changes in luminescence dating of waterlain deposits. *Geochronometria* **30**, 33-40.

Murray, A.S., Olley, J.M. 2002. Precision and accuracy in the optically stimulated luminescence dating of sedimentary quartz: a status review. *Geochronometria* **21**, 1-16.

Murray, A.S., Wintle, A.G. 2000. Luminescence dating of quartz using an improved single-aliquot regenerative-dose protocol. *Radiation Measurements* **32**, 57-73.

Olley, J.M., Caitcheon, G., Murray, A.S. 1998. The distribution of apparent dose as determined by optically stimulated luminescence in small aliquots of fluvial quartz: implications for dating young sediments. *Quaternary Geochronology* **17**, 1033-1040.

Olley, J.M., Reed, M. 2003. *Radial Plot 1.3*, CSIRO Land and Water.

Prescott, J.R., Clay, R.W. 2000. Cosmic ray dose rates for luminescence and ESR dating: measured with a scintillation counter. *Ancient TL* **18(1)**, 11-14.

Prescott, J.R., Hutton, J.T. 1994. Cosmic ray contributions to dose rates for luminescence and ESR dating: large depths and long-term time variations. *Radiation Measurements* **23**, 497-500.

Prescott, J.R., Hutton, J.T. 1995. Environmental dose rates and radioactive disequilibrium from some Australian luminescence dating sites. *Quaternary Science Reviews* **14**, 439-448.

Prescott, J.R., Hutton, J.T. 1987. Low level measurements of potassium, thorium and uranium by means of scintillometry in the field. *Proceedings, Fifth Australian Conference on Nuclear Techniques of Analysis, Lucas Heights, AINSE, Sydney*, 76-78.

Prescott, J.R., Robertson, G.B. 1997. Sediment dating by luminescence: a review. *Radiation Measurements* **27(5/6)**, 893-922.

Walker, M. 2005. *Quaternary dating methods: an introduction*. John Wiley & Sons.

Wintle, A.G., Murray, A.S. 2006. A review of quartz optically stimulated luminescence characteristics and their relevance in single-aliquot regeneration dating protocols. *Radiation Measurements* **41**, 369-391.

2.2 Accelerator Mass Spectrometry radiocarbon dating

'A fool sees not the same tree that a wise man sees' – William Blake

Radiocarbon dating is the oldest radiometric dating method with its fundamental concept formulated in the aftermath of WWII (Libby 1946). It is based on the radioactive carbon isotope carbon-14 (^{14}C) which is formed in the upper atmosphere through neutron bombardment of nitrogen by cosmic rays. Carbon-14 rapidly oxidises to $^{14}CO_2$ and disseminates throughout the atmosphere, hydrosphere and biosphere, while slowly decaying to nitrogen-14 (^{14}N) and beta radiation (formula [1] in Libby 1952). The radioactive decay is compensated by a steady production, resulting in a near-equilibrium throughout the global carbon cycle. Plants fix an equivalent fraction of $^{14}CO_2$ during photosynthesis and are consumed by other organisms. Hence, ^{14}C can be found in all living matter in a near-equal concentration, or as Libby puts it "*Since plants live off the carbon dioxide, all plants will be radioactive; since the animals on earth live off the plants, all animals will be radioactive. Thus we conclude that all living things will be rendered radioactive by the cosmic radiation.*" (Libby 1952). Death results in isolation from the global carbon cycle, followed by an exponential depletion of radiocarbon which has a half life of ~5568 a (Arnold & Libby 1951). Radiocarbon dating measures the residual activity or concentration of ^{14}C and compares it to that of living organisms, thereby making it possible to infer the time of isolation, i.e. the radiocarbon age (see formula [5] in Libby 1952).

Conventional radiocarbon dating determines the ^{14}C-activity by measuring the count rate of beta radiation. Since the late seventies, an analytical breakthrough in trace element analysis made it possible to directly measure ^{14}C-concentrations, more specifically to differentiate it from ^{14}N with a similar charge-to-mass ratio (Bennett et al. 1977; Muller 1977). This is achieved by accelerating the carbon particles (in form of negatively ionised graphite) to high energies and measuring isotope-dependent ionisation rates. The main advantage of atom counting by mass spectrometry over decay counting is an improved efficiency in the order of three magnitudes. In terms of sample quantity requirements, this translates to less than a tenth of a milligram of carbon instead of the few grams required for conventional radiocarbon dating, which in turn allows for a more targeted selection of samples and rigorous pre-treatment. The precision of AMS radiocarbon dating is better than 1 % and reflects the combined errors and uncertainties from counting statistics, standards, measurements and the natural background (Beukens 1992). It is expressed either as one (68.27 %) or two (95.45 %)

standard deviations from the best AMS-age estimate. The detection limit of ^{14}C and thereby radiocarbon dating is generally given as eight half lives; i.e. ~46 ka BP (Walker 2005).

Ages are presented in radiocarbon years before present (BP = 1950). Natural short- and long-term variations in global ^{14}C-concentration result in discrepancies with calendar years and require calibration with an independent numerical dating method. Further, plants preferably take up the lighter carbon isotopes ^{12}C and ^{13}C resulting in variation in the equilibrium distribution of the $^{14}C/^{12}C$-ratio. This isotopic fractionation is largely dependent on the photosynthetic pathway of the plant species and results in variable depletion of radiocarbon. The correction is based on the principle that fractionation between ^{14}C and ^{12}C is approximately double that of the stable isotopes ratio $^{13}C/^{12}C$ which can easily be measured. Comparison of the isotopic composition with a standard allows for normalisation and is conducted by the radiocarbon facility as a standard correction (Gupta & Polach 1985).

Sample-specific sources of error

In radiocarbon dating, contamination refers to any alteration of the $^{14}C/^{12}C$-ratio after death of the organism other than radioactive decay. It is often difficult to detect, gauge and correct and there is a great number of mechanical, chemical and microbiological post-depositional processes with such potential. Old samples with low residual ^{14}C-activity are particularly susceptible to contamination by modern material. The laboratory approach to this problem is sample material- and context-specific, with the general aim to reduce the sample to the one carbon component most likely referring to the event to be dated (Hedges 1992).

In any stratigraphic context the implicit assumption of concurrence of the radiocarbon-dated material and depositional event is made. However, it has long been demonstrated for fluvial deposits that this does not necessarily hold true (Blong & Gillespie 1978). Confidence in the reliability of a ^{14}C-based chronostratigraphy can be significantly increased by pairing radiocarbon dates based on different sample materials and with independent numerical dating methods such as luminescence dating.

Charcoal and charred plant macrofossils:

Discrete charcoal pieces (see Fig. 2.2A) are generally considered the preferred sample material in terms of laboratory treatment and radiocarbon dating due to its high inert carbon content and relative low contamination risk (Hedges 1992). However, owing to its high surface area charcoal also has a strong adsorption potential of environmental contaminants and often comprises a wide spectrum of impurities. The standard pre-treatment procedure consists of an iterative acid-alkali-

acid (AAA) treatment; hot hydrochloric acid is used to eliminate secondary carbonates and for final neutralisation after warm alkali washes (NaOH) to flush out humic adsorbents. The very longevity of charcoal allows it potentially to endure multiple cycles of sediment storage, erosion and re-deposition, presenting a considerable interpretative challenge in terms of the significance of the obtained age in a stratigraphic context (Blong & Gillespie 1978).

Fig. 2.2A) *Large discrete piece of charcoal (sample OZJ904 from BRA07-SD)*

In addition to discrete charcoal pieces, veneers of charred organic detritus were sampled from laminated stratigraphic sections (see Fig. 2.2B). The potential spectrum of burned and degraded plant macrofossils is wide and hence problematic. However, the organic veneers readily disintegrate in water. While this creates procedural difficulties, it also presents interpretative advantages over discrete charcoal pieces in that such fragile components are unlikely to survive reworking.

Fig. 2.2B) *Dark veneers of organic detritus partly covered by tufa precipitation as seen from the top and side (indicated).*

Carbonate shells:

Another type of material sampled for radiocarbon dating consists of small carbonate shells from aquatic gastropods (see Fig. 2.2C). Carbonate shells are generally perceived as problematic since the gastropods feed on sub-aquatic plants not necessarily in equilibrium with the atmospheric radiocarbon concentration. In the vicinity of groundwater discharge containing dissolved carbonates from limestone formations the aquatic fauna is likely to ingest “dead” carbon. Finally, shells are prone to diagenetic re-crystallisation with soil carbonates (Walker 2005). However, contamination of carbonate shells very much depends on the geological and depositional environment and preservation. Contamination with pedogenic calcite can easily be differentiated from the aragonite shells by X-ray diffraction and eliminated by the standard chemical pre-treatment procedure removing everything but the core of the shell by acid hydrolysis (Gupta & Polach 1985). As with charcoal pieces, shells have the potential to survive erosion and re-deposition, especially when transported in suspension or by soil creep. However, the degree of fragmentation can be more readily assessed and broken shell fragments excluded from the bulk sample during physical pre-treatment.

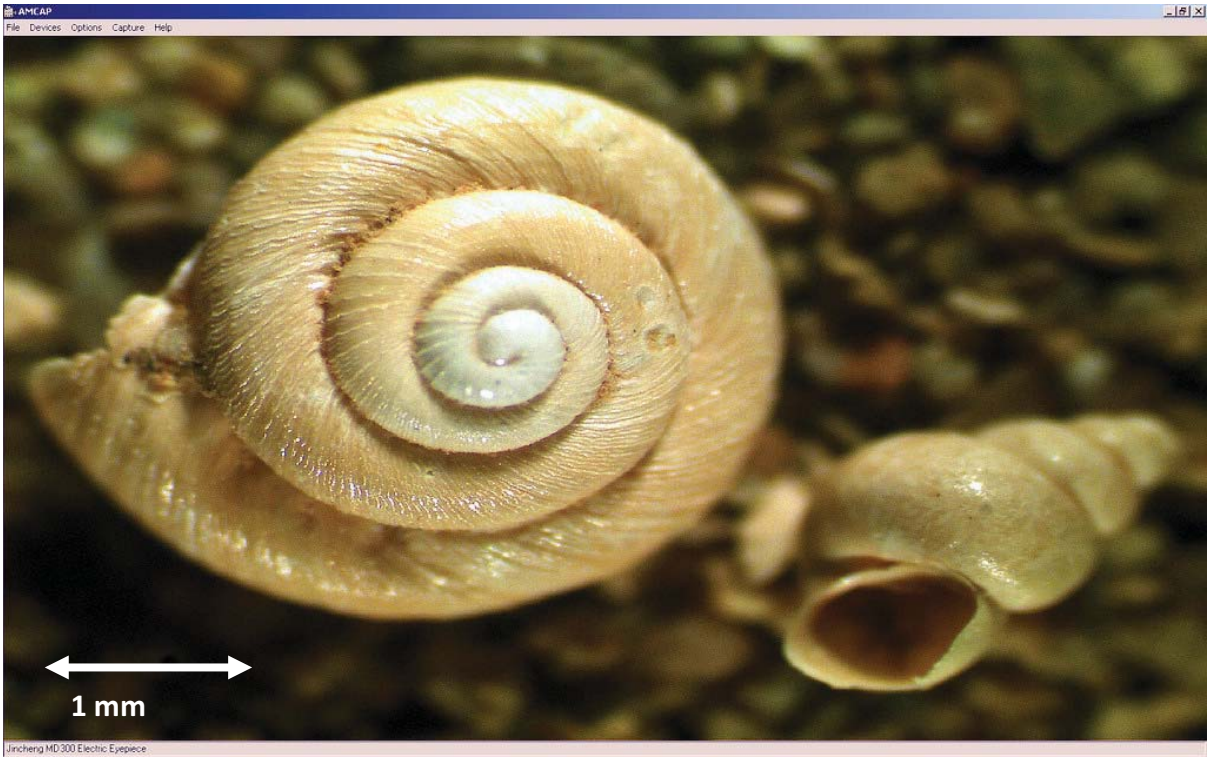

Fig. 2.2C) *Carbonate gastropod shell sample [Charopidae sp. (left) and Austropyrgus sp. (right)] from the basal unit of BRA-SD prior to chemical pre-treatment.*

Calibration

It has early been recognised that the global ^{14}C-concentration fluctuated over the past ~46 ka and at times diverged sharply from the measured historic concentrations (de Vries 1959). Long-term variations are caused by modulations of the cosmic ray flux linked to variations in the earth´s magnetic field and solar activity affecting the ^{14}C-production rate, and by changes of the reservoir capacity of oceans, rivers and lakes reflecting climate-related impacts on vertical mixing (Hughen et al. 2004). Radiocarbon concentrations are elevated throughout most of the effective time range of radiocarbon dating, particularly during the LGM and its lead-up. This results in considerable underestimation in terms of calendar years. The non-linear offset therefore requires calibration with an independent numerical dating method such as annual tree-rings (Ferguson et al. 1966) now extended to ~12.4 ka, and varved marine sediments extended to ~14.7 ka (Reimer et al. 2004). Beyond, ^{14}C- and ^{230}Th-dated fossil corals provide a marine-based calibration of less precision (Fairbanks et al. 2005). A high-resolution marine-derived ^{14}C-dated sedimentological and geochemical record from Cariaco Basin, initially correlated to Dansgaard-Oeschger events recorded in the Greenland GISP2 ice core (Hughen et al. 2004) and now tied to the high-resolution ^{230Th}-dated Hulu Cave speleothem record, provides the latest improvement in terms of reliability and precision (Hughen et al. 2006). The updated Cariaco results are in good agreement with independent

fossil coral records (e.g. Fairbanks et al. 2005) and employed in the CalPal-2007$_{Hulu}$-calibration data set (Weninger & Jöris 2008) as part of the CalPal-2007 calibration and palaeoclimate research software package (Weninger et al. 2008), used in this study to calibrate all ^{14}C-ages. Despite recent advances, uncertainties in calibrating the older half of the ^{14}C time scale remain (Hoffman et al. 2008). As a result, the error margin is here presented as two standard deviations and calibrated dates are expressed as a range between minimum and maximum ages before 1950 (cal BP). Abrupt large shifts in ^{14}C-concentration beyond 28 ka cal BP result in prolonged "age plateaus", reflected in large error ranges (see Fig. 2.2D).

AMS data discussion

The chronostratigraphic description, interpretation and discussion of the Flinders Silts are based on 93 AMS samples from 14 stratigraphic type sections (section 3.1). In addition to the 30 OSL samples, 43 radiocarbon dates were obtained within the scope of this PhD study; 27 by Single Stage Accelerator Mass Spectrometry (SSAMS) at the Australian National University (ANU) in collaboration with the Cooperative Research Centre for Landscape Environments and Mineral Exploration (CRC LEME), 11 in collaboration with the AMS facility at the Australian Nuclear Science and Technology Organisation (ANSTO) at Lucas Heights, and five commissioned to the Waikato radiocarbon facility in New Zealand. The remainder is re-calibrated from published reports (23 in Cock et al. 1999 and Williams et al. 2001) or presented in co-authorship with Martin A. J. Williams (14) and Peter Glasby (13).

The individual AMS dates are best discussed for each stratigraphic type section respectively. However, some overall observations concerning the reliability of different sample material in terms of chronostratigraphic significance are best made in the form of a synopsis. Below, all AMS-dates from the Flinders Silts are plotted as a function of depth below the top of respective stratigraphic sections and sample material (see Fig. 2.2D). Despite this rough comparative approach, some observations made in most individual stratigraphic sections are well illustrated for the whole set. Firstly, the dates obtained from carbonate shells and veneers of organic detritus correlate reasonably well along an approximately linear trend. This suggests similar deposition rates and concurrent termination of the fine-grained aggradational sequences across a range of geomorphologic settings and different catchments. In contrast, charcoal-derived ages are scattered in relation to depth. Dates both older than 30 ka cal BP and younger than 18 ka cal BP are derived from sample depths ranging from 25 to 1,300 cm below top. Throughout the LGM, they largely deviate from the approximate general chronostratigraphic trend of AMS-ages based on shells and organic veneers. This observation is supported by individual pieces of charcoal sampled from organic

veneers that returned much older ages presenting outliers in the respective chronostratigraphic sequences. In conclusion, radiocarbon ages derived from charcoal in the studied depositional environment must be treated strictly as *post quem* dates in any stratigraphical context. While they represent a problematic proxy for dating depositional events, charcoal pieces are to some degree of palaeo-environmental significance for their cumulative occurrence is likely to reflect the presence of woody vegetation and wildfires within the catchment.

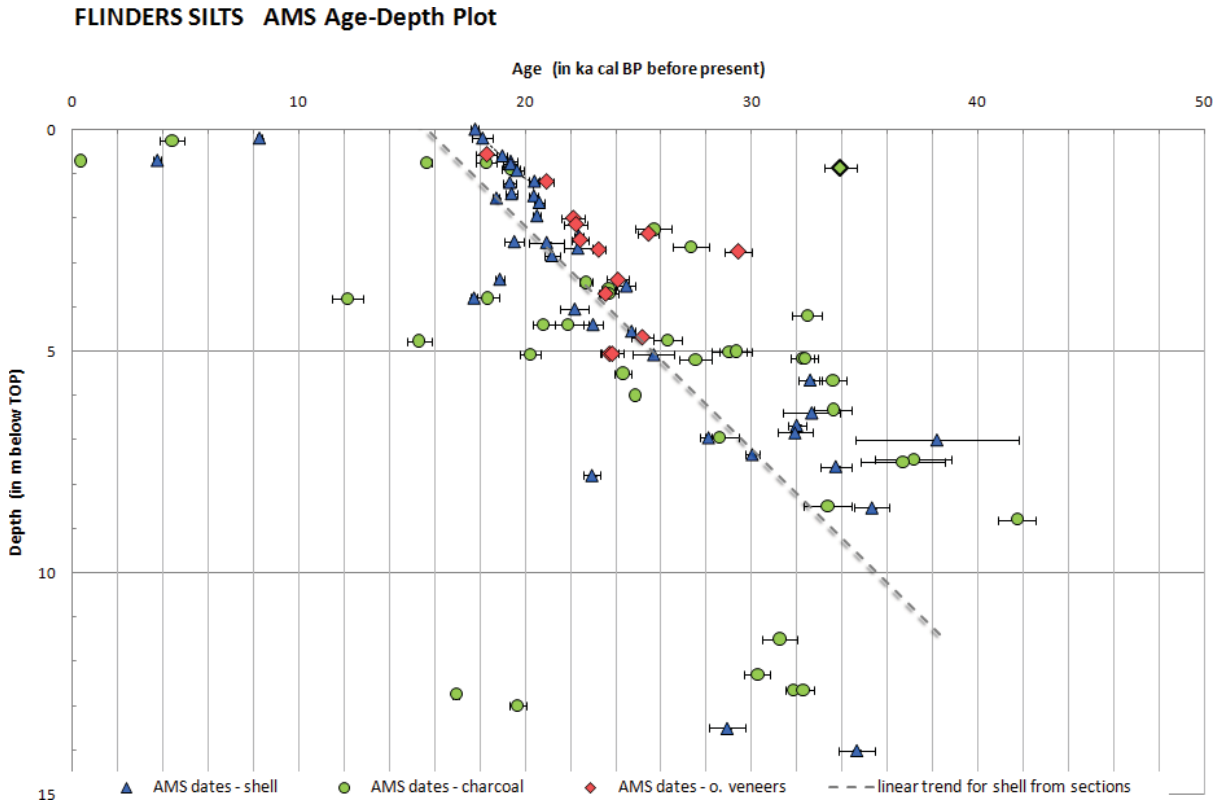

Fig. 2.2D) *Flinders Silts calibrated radiocarbon data colour-coded by sample material: carbonate shells (blue triangles); charcoal pieces (green circles); veneers of plant detritus (red diamonds). The linear regression for the shell samples is indicated by the dotted line.*

References

Arnold, J.R., Libby, W.F. 1951. Radiocarbon dates. *Science* **113**, 111-120.

Bennett, C.L., Beukens, R.P., Clover, M.R., Gove, H.E., Liebert, R.B., Litherland, A.E., Purser, K.H., Sondheim, W.E. 1977. Radiocarbon dating using electrostatic accelerators: negative ions provide the key. *Science* **198**, 508-510.

Beukens, R.P. 1992. Radiocarbon Accelerator Mass Spectrometry: background, precision and accuracy. In: Tayler, R.E., Long, A., Kra, R.S. (eds.), *Radiocarbon after four decades: an interdisciplinary perspective*. Springer, pp. 230-239.

Blong, R.J., Gillespie, R., 1978. Fluvially transported charcoal gives erroneous ^{14}C ages for recent deposits. *Nature* **271**, 739-741.

Cock, B.J., Williams, M.A.J., Adamson, D.A. 1999. Pleistocene Lake Brachina: a preliminary stratigraphy and chronology of lacustrine sediments from the central Flinders Ranges, South Australia. *Australian Journal of Earth Sciences* **46**, 61-69.

Fairbanks, R.G., Mortlock, R.A., Chiu, T.-C., Cao, L., Kaplan, A., Guilderson, T.P., Fairbanks, T.W., Bloom, A., Grootes, P.M., Nadeau, M.-J. 2005. Radiocarbon calibration curve spanning 0 to 50,000 years BP based on paired $^{230Th/234U/238}U$ and ^{14}C dates on pristine corals. Quaternary Science Reviews **24**, 1781-1796.

Ferguson, C.W., Huber, B., Suess, H.E. 1966. Determination of the age of Swiss lake dwellings as an example of dendrochronologically-calibrated radiocarbon dating. *Zeitschrift für Naturforschung Teil A* **21(34)**, 1173-1177.

Gupta, S.H., Polach, H.A. 1985. *Radiocarbon dating practices at ANU*. Canberra, Australian National University Press.

Hedges, R.E.M. 1992. Sample treatment strategies in radiocarbon dating. In: Tayler, R.E., Long, A., Kra, R.S. (eds.), *Radiocarbon after four decades: an interdisciplinary perspective*. Springer, pp. 165-183.

Hoffman, D.L., Beck, J.W., Richards, D.A., Smart, P.L., Mattey, D.P., Paterson, B.A., Hawkesworth, C.J. 2008. Atmospheric radiocarbon variation between 44 and 28 ka based on U-series dated speleothem. *Geophysical Research Abstracts* **10**.

Hughen, K., Southon, J., Lehman, S., Bertrand, C., Turnbull, J. 2006. Marine-derived ^{14}C calibration and activity record for the past 50,000 years updated from the Cariaco Basin. *Quaternary Science Reviews* **25**, 3216-3227.

Hughen, K., Lehman, S., Southon, J., Overpeck, J., Marchal, O., Herring, C., Turnbull, J. 2004. ^{14}C activity and global carbon cycle changes over the past 50,000 years. *Science* **303**, 202-207.

Libby, W.F. 1946. Atmospheric helium three and radiocarbon from cosmic radiation. *Physical Review* **69**, 671-672.

Libby, W.F. 1952. *Radiocarbon dating, 1st ed*. Chicago, U.S.A., The University of Chicago Press.

Muller, R.A. 1977. Radioisotope dating with a cyclotron. *Science* **196**, 489-494.

Reimer, P.J., Baillie, M.G.L., Bard, E., Bayliss, A., Beck, J.W., Bertrand, C.J.H., Blackwell, P.G., Buck, C.E., Burr, G.S., Cutler, K.B., Damon, P.E., Edwards, R.L., Fairbanks, R.G., Friedrich, M., Guilderson, T.P., Hogg, A.G., Hughen, K.A., Kromer, B., McCormac, F.G., Manning, S.W., Ramsey, C.B., Reimer, R.W., Remmele, S., Southon, J.R., Stuiver, M., Talamo, S., Taylor, F. W., van der Plicht, J., Weyhenmeyer, C.E. 2004. IntCal04 atmospheric radiocarbon age calibration, 26-0 cal kyr BP. *Radiocarbon* **46**, 1029-1058.

de Vries, H.L. 1959. Variation in concentration of radiocarbon with time and location on Earth. In: Abelson, P.H. (ed.), *Researches in Geochemistry*. New York, John Wiley & Sons, pp. 180.

Walker, M., 2005. *Quaternary dating methods: an introduction*, John Wiley & Sons.

Weninger, B., Jöris, O. 2008. A ^{14}C age calibration curve for the last 60 ka: the Greenland-Hulu U/Th timescale and its impact on understanding the Middle to Upper Paleolithic transition in Western Eurasia. *Journal of Human Evolution* **55(5)**, 772-781.

Weninger, B., Jöris, O., Danzeglocke, U. 2008. CalPal-2007. *Cologne Radiocarbon Calibration & Palaeoclimate Research Package*. Available at: http://www.calpal.de/ [Accessed July 28, 2008].

Williams, M.A.J., Prescott, J.R., Chappell, J., Adamson, D., Cock, B., Walker, K., Gell, P. 2001. The enigma of a late Pleistocene wetland in the Flinders Ranges, South Australia. *Quaternary International* **83-85**, 129-144.

2.3 Particle-Size Analysis

'Great things are done by a series of small things brought together' – Vincent van Gogh

The largely structureless and homogenous nature of the fine-grained valley-fill deposits limits the potential of field texturing and sedimentological observations for inferring former depositional environments. Apart from rare faint current cross-bedding structures observed in sandy intercalated beds, and more common imbricated gravel exposures of clast-supported cut-and-fill structures, the fine-grained sediments themselves offer little clue to the interpreter. Field texturing invariably returns silty to sandy loam, sometimes becoming heavier with kneading. This texture change is widely reported in south-eastern Australia from soils associated with loess mantles (e.g. Beattie 1970; McIntyre 1976). Butler introduced the term 'subplasticity' to describe the phenomenon which reflects the presence of clay aggregates resisting mechanical dispersion (Butler 1955; Butler 1976).

In order to address the lack of macroscopic sedimentary structures and the deficiencies of field texturing, high-resolution laboratory particle-size analysis (PSA) was performed. The two most important objectives hereby addressed are the inferred aeolian provenance of the material, and the former modes of transport and deposition. The layered to laminated stratigraphic section BRA-AR (Fig. 2.3A) at the confluence of the Aroona and Brachina Creeks was selected for a detailed study on vertical particle size-trends, in order to establish the depositional processes behind observed stacked laminations similar to those discussed for stratigraphic section BRA-SD (section 3.2).

In order to decide whether the sediment samples should be sized in their naturally-occurring partially-aggregated condition or in a fully-dispersed state, it proved imperative to first resolve if the aggregates are a pre- or a post-depositional phenomenon. In other words, it needed to be established if the sediments were transported as sand-sized aggregates (Schieber et al. 2007), in which case they can be assumed to record the size- and density-dependent sorting processes, or if the aggregates are the product of in-situ pedogenic processes (Rust and Nanson 1989), in which case they would obscure the sought-after information. The difficulties faced in sizing partially-aggregated sediments are best illustrated by a quote from Dare-Edwards: '... there is no correct particle size distribution for subplastic samples, only a pattern that corresponds to the (dispersion) technique used' (1982; 181). However, a large number of previous studies addressed disaggregation of subplastic sediments, providing dispersion protocols (e.g. McIntyre 1976; Norrish and Tiller 1976; Chittleborough 1982).

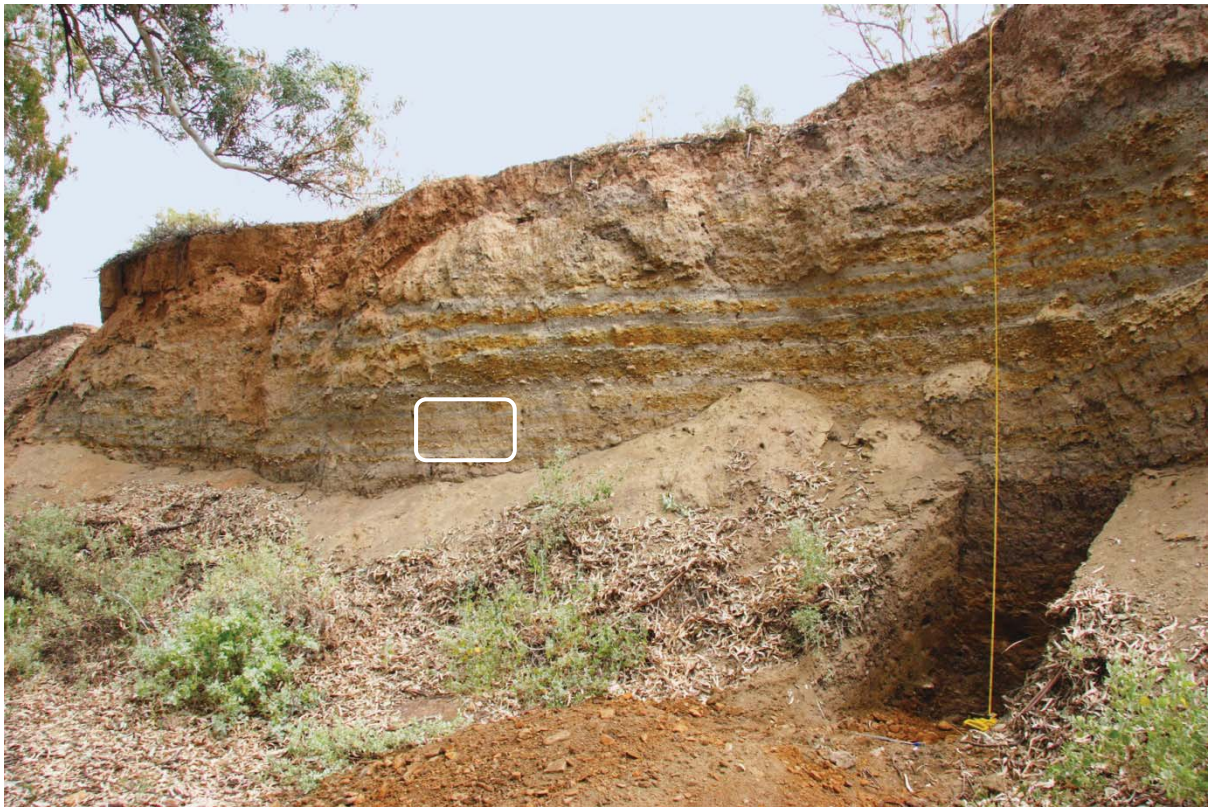

Fig. 2.3A) *Layered to laminated stratigraphic section BRA-AR situated few meters upstream of the present confluence of the Aroona Creek tributary with the Brachina Creek trunk channel. The studied interval of laminations is indicated.*

The narrow size-range and subtle differences between the individual samples called for a particle-sizing technique particularly adapted to silt-sized sediments; providing exceptional high resolution, and the largest possible number of discriminated size classes (Goossens 2008). The employed Multisizer™ 3 COULTER COUNTER®, based on the electrical sensing zone principle (Beckman Coulter 2002), proved ideal for the scope of this study (McTainsh et al. 1997). In collaboration with Grant McTainsh, the latest instrument and an array of aperture tubes specifically selected for the study of dust-derived sediments (560, 280, 140 and 50 µm) were used over repeated laboratory visits to the Australian School of Environmental Studies at Griffith University, Brisbane. Sample preparation and sizing protocols were adapted from McTainsh et al. (1997), and further developed as described in detail in appendix 5.2.3.1. The particle-size distributions (PSD) were analysed using a parametric statistical approach inspired by Leys et al. (2005). Reported shortcomings, such as restricted data resolution and limited control on curve-fitting algorithms, were addressed by using the open source "Mixdist" library (Macdonald & Du 2004) within the "R environment for statistical computing" (R Foundation 2008). Finally, an original protocol allowing the comparison of partially-aggregated with fully-dispersed samples was developed (appendix 5.2.3.2). The methodological advances of the

sediment-sizing study were deemed important enough to be presented as a separate paper. The following manuscript provides a review of the historical development of statistical approaches towards analysing PSDs, the new protocol allowing quantification of size distributions and relative abundances of aggregates within samples, and the results for the studied laminations of stratigraphic section BRA-AR (Fig. 2.3B). Detailed protocols are presented in appendices 5.2.3, 5.2.3.1 and 5.2.3.2.

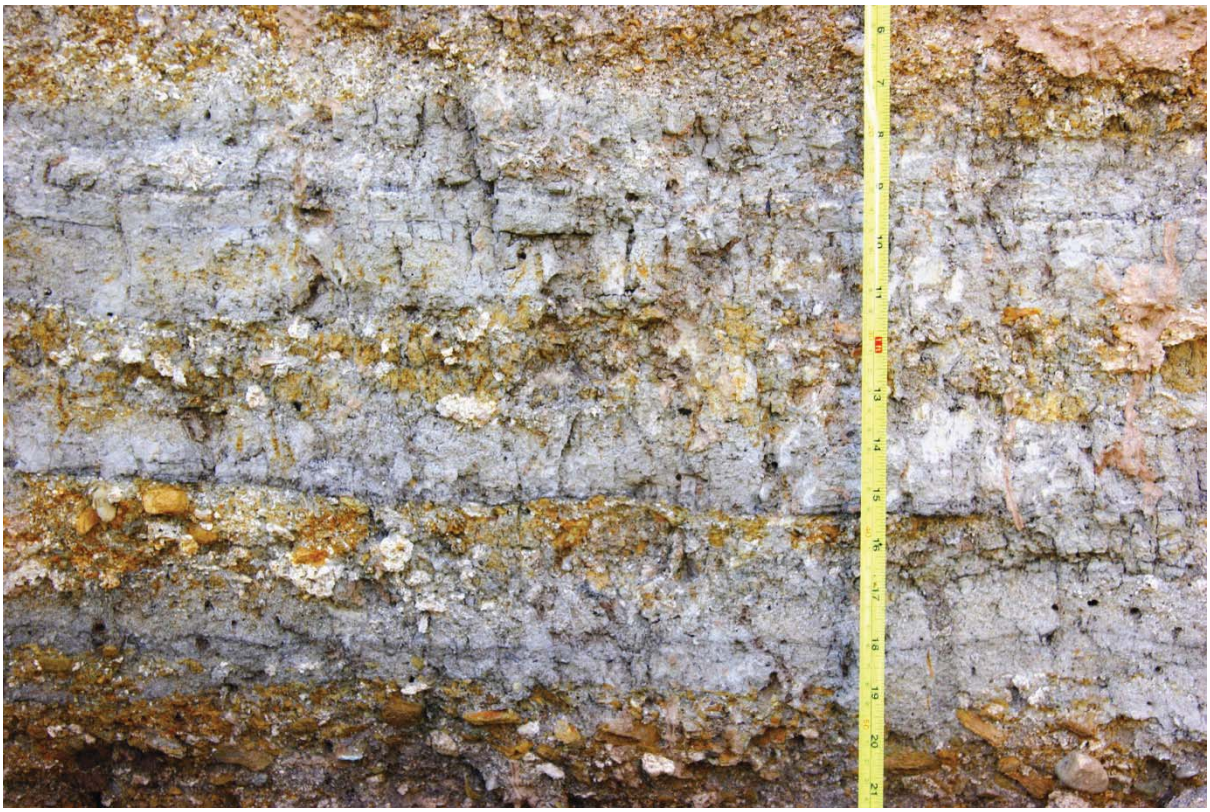

Fig. 2.3B) *Laminations of the studied sub-section of BRA-AR, intercalated with orange-mottled gravel sheets and white clasts of local spring tufa.*

Quantifying particle aggregation in fluvial sediments

(similar version in revision with Sedimentology)

David Haberlah [1, 2], Grant H. McTainsh [3]

1) School of Earth and Environmental Sciences, University of Adelaide, Adelaide, SA 5005, Australia

2) Cooperative Research Centre for Landscape Environments and Mineral Exploration

3) *Griffith School of Environment, Griffith University, Brisbane, QLD 4111, Australia*

Abstract

Sediments largely occur as non-normal size distributions composed of discrete, partially-aggregated particle populations. These populations reflect provenance, dispersal pathways and their depositional environments. The experimental laboratory studies by Schieber and co-authors (*Science* **318,** 2007) describing mud flocculation in turbulent marine systems, prompted us to investigate the potential of aggregates to record size-sensitive depositional processes in a terrestrial fluvial system. Here we use decompositional statistical analysis of sediment-size distributions in their natural condition of particle-aggregate mixtures, which has not been attempted before. We outline and field test a practical and freely-available parametric approach which allows a sediment to be viewed in both its conventional particulate form and as a naturally-occurring mixture of transport-stable aggregates and particles. We also demonstrate that it is only by quantifying aggregation that the provenance and depositional processes forming sediments with complex fluvial and aeolian origins can be understood.

Keywords:

aggregation, particle-size analysis, grain-size analysis, component population analysis, decomposition, mud aggregates.

Introduction

The earth's surface is covered by sediments and soils composed of mixtures of elementary particles and aggregates. It is well established that parent rocks and weathering processes determine the range of particle sizes and that the size-selective processes of entrainment, transport and deposition by water and wind control the particle-size distribution of the resultant sediments (Udden 1914). The study of particle-size distributions therefore has the potential to unlock the provenance and geomorphic history of sediments. While a large number of particle-size studies have significantly improved our understanding of the formation of deposits from around the world, they have not realised their full potential because of their narrow focus upon elementary particles at the expense of aggregates.

Recent flume experimental studies have provided a paradigm shift in our understanding of how mudstones are formed, by demonstrating that mud aggregates flocculate in turbulent marine conditions (Schieber et al. 2007). This observation obliges earth scientists to fundamentally review their long-held assumption that mudstones reflect low energy, usually deep offshore marine environments. These flume studies however stop short of providing a method to measure aggregate-size. In the present study, we come to a similar conclusion about the importance of aggregates in turbulent fluvial terrestrial environments, and demonstrate a method that describes and quantitatively resolves their presence in natural sediments. Based on a field study of flood deposits in the Flinders Ranges, South Australia, we present an innovative approach to sediment-size analysis (as distinct from particle-size analysis) and show that measuring aggregate populations within sediment-size distributions provides new perspectives on the formation of fluvial and aeolian deposits.

Review of earlier studies

There are two main reasons why sediment-size studies have focused upon particle size at the expense of aggregate-size, and these relate to laboratory sizing methods and the statistical analysis of size data. Because of practical constraints on traditional laboratory particle-size analysis, the vast majority of studies have been performed on sediment samples in a dispersed particulate condition. Traditional particle-size analysis involves multiple steps and different methods; such as dry and wet-sieving of the sand-sized fraction (>62.5 μm), and the use of a pipette or sedimentation balance for the finer silt- (62.5-3.9 μm) and clay- (<3.9 μm) sized fractions. The exposure of partially-aggregated sediments to such diverse analytical procedures results in uncontrolled breakup of mud aggregates

at different steps in the analysis; with unpredictable impacts on resultant size distributions. Aggregates pose an additional problem in analyses where particle size is estimated from settling velocity based on Stokes' Law, by not complying with the basic requirement for an overall uniform particle density. The specific density of quartz, which is commonly assumed for elementary particles, significantly over-estimates that of mud aggregates. Conventional sample pre-treatment protocols therefore involve physical and chemical dispersion of sediments into elementary particles that will remain unaltered during the sizing process. With the introduction of sophisticated sediment-sizing instruments based upon the principles of electrical sensing, light and laser diffraction, fine sediment samples can now be sized using a single method (Goossens 2008). These instruments significantly reduce uncontrolled disaggregation during size analysis and circumvent the need for the uniform density assumption. As a result, sediments can be analysed in a variety of sample conditions ranging from minimally-dispersed/ partially-aggregated to fully-dispersed/ particulate conditions, simply by changing the sample pre-treatment (McTainsh et al. 1997).

The second reason why sediment-size studies have focused upon particle size at the expense of aggregate-size, relates to past limitations in our capacity to statistically analyse complex particle-size distributions (PSDs). To explain this, a brief overview of the history of statistical particle-size data analysis is presented. Udden (Udden 1898) and Wentworth (Wentworth 1922) were among the first to conclude that PSDs are best presented on log-normal scale, emphasising changes in ratios between size classes rather than their absolute differences. It was early recognized that well-sorted sediments approximate log-normal size distributions, taking up the classic Gaussian bell-shape in a log-normal frequency histogram, or a straight line in a cumulative plot (Richardson 1903) (Otto 1939). This paradigm shift was however soon tempered by the realisation that most sediments depart from this "ideal", giving rise to asymmetric or polymodal PSDs in frequency histograms, and multiple straight segments forming "zig-zag lines" in cumulative plots. During the forties and fifties, such deviations were recognised to reflect mixtures of discrete sedimentary populations that can be approached in three fundamental ways. **1)** (Inman 1952) and (Folk & Ward 1957) statistically characterised departures from log-normality of the total-sample PSD by developing a range of graphical measures of mean size, sorting, skewness and kurtosis statistics. **2)** (Bagnold 1937) and others (Bagnold & Barndorff-Nielsen 1980)) looked for alternative distribution functions that match particular PSDs best. However, in the early sixties McCammon (McCammon 1962) demonstrated that statistical descriptions of multi-component PSDs are potentially misleading, pointing towards an earlier conceptual approach of **3)** resolving PSDs into discrete component populations (CPs) (Bagnold 1941) (Doeglas 1946) (Crocker 1946). In these pre-computer days, researchers faced considerable practical data analysis obstacles. All early graphical, *i.e.* (Sindowski 1957) (Harris 1958) (Tanner 1958)

(Walger 1962) (Fuller 1962) (Spencer 1963) (Visher 1969), and numerical (Clark 1976) decompositional PSD studies were limited to dissecting cumulative curves at “break points” into multiple truncated Gaussian components, despite Bagnold’s early statement that frequency histograms are ‘clearly preferable for the more practical reverse process of finding the regular components of a [sediment] sample’ (Bagnold 1941):119). In the early seventies, a significant advance was made by Folk in Australia (Folk 1971), by graphically decomposing PSDs in the more realistic scenario of a series of overlapping log-normal curves corresponding to discrete CPs. This approach was followed by a decade of qualitative inverse modelling using the “Du Pont 310 Curve Resolver”, an analogue computer capable of graphically resolving and quantifying overlapping log-normal CPs in polymodal frequency histograms (Oser 1972) (van Andel 1973) (Dauphin 1980). Possibly due to the requirement of expensive dedicated hardware, a more widespread application was not realised despite the genetically meaningful results of these pioneering studies.

With the spread of desktop computers, more rigorous parametric approaches based on analytical inverse curve-fitting models became available, calculating best-fitting sets of continuous unimodal probability distributions (Sheridan et al. 1987). At present, there has been a small number of pioneering decompositional analytical studies that have demonstrated the potential of the method, by accurately decomposing known synthetic complex particle mixtures (Leys et al. 2005), and showing how understanding of the provenance of a wide range of sediments can be improved (Sun et al. 2002). However, these published statistical software solutions either remain commercially unavailable (private VBA script in case of (Sun et al. 2002), or depend on outdated operating systems (DOS in case of Leys *et al.*, 2005) and are restricted by limitations on size-class data.

In the present study, we use the public domain “Mixdist” library (Macdonald & Du 2004) which is part of the “R” environment for statistical computing (R Development Core Team 2008) distributed online via CRAN. “Mixdist” was originally developed for ecological population studies (Macdonald & Green 1988) and can be adapted to other needs under the GNU General Public License. Based on the method of maximum likelihood, “Mixdist” fits finite mixture distribution models to grouped and conditional data using a Newton-type and the Expectation-Maximization algorithms.

Site and Samples

In the present study, we sampled the vertical face of a layered, fine-grained and partially-aggregated alluvial terrace remnant at the confluence of the Brachina and Aroona Creeks in the semi-arid Flinders Ranges of South Australia (S 31.329°/ E 138.586°). Mouths of tributary streams are often back-flooded by trunk streams, resulting in a layered succession of sediments, referred to as

slackwater deposits (Kochel & Baker 1982). A series of flood events can produce stacked fining-upward flood couplets which reflect the differential size-, and density-sensitive settling of sediments from a suspension. Typically, fine-grained bands within such couplets reflect multiple fluxes of sediment, separated by dark veneers of organic flotsam plus sediment (Kochel & Baker 1988). As such, slackwater deposits provide an excellent opportunity for detailed analysis of vertical size-trends. Within a continuous succession of three, complex but largely undisturbed flood couplets, six light bands topped by five dark bands were sampled (see appendix 5.2.3). The dark bands display multiple veneers of plant detritus, interpreted as organic flotsam which has settled out of suspension last, and the associated sediments are assumed to be finer than those in the underlying light bands. The largely undisturbed laminated nature of the veneers indicates minimal post-depositional disturbance.

Methodology

The Coulter Multisizer 3™ used to analyse these samples emulates a turbulent fluvial environment during the sizing-process (Beckman Coulter 2002). Samples are immersed in a weak electrolyte (1% NaCl), required for the electrical sensing zone principle to operate, and stirred in a baffled beaker to maintain a uniform suspension. This inevitably breaks up loosely-bound aggregates, but samples quickly reach a stable state in which further dispersion is resisted. This we describe as its transport-stable condition, because such a sample would survive transport in non-laminar water flow. Subsequently, we fully disperse the sample into its particulate condition. Physical pre-treatment consists of an ultrasonic bath (Branson 2200 sonifier, 472Hz/ 60W for 30 minutes). Chemical pre-treatment consists of removing carbonate cementation in hydrochloric acid (1% HCl). Calgon (a standard dispersant) is not added since this resulted in flocculation of the sample suspension. Reproducibility of laboratory results is confirmed here for both pre-treatment protocols by time-transgressive test runs and from inspection of samples by binocular microscope (Fig. 1A and D). As the Coulter Multisizer 3™ requires only very small quantities of sample, the continuous vertical succession of centimetre-thin bands within the slackwater deposit could be analysed. The size distributions of each band are based on more than a million individual particle-size counts and volume measurements, numerically merged by the Beckman Coulter Multisizer software (v.3.51) into 256 discrete size classes (see appendix 5.2.3).

Decompositional sediment-size analysis (referred to here as Component Population Analysis - CPA) is performed on both minimally- and fully-dispersed size distributions of the fluvial sediments. This parametric analysis is initiated in unconstrained modus, specifying three hypothetical evenly-spaced Gaussian end-member populations as starting points of the computation. There is no compelling

reason to limit CPA to Gaussian distributions. In fact, it has long been demonstrated for the more readily-sizable gravel fraction in fluvial systems that component populations (CPs) are best described by the stretched-exponential Weibull (Rosin) distribution (Krumbein & Tisdel 1940) (Ibbeken 1983) (Kondolf & Adhikari 2000), a claim more recently made for disaggregated fine sediments from a variety of environments (Sun et al. 2002). The process is hence repeated for Weibull distributions, and statistics are compiled for both sample expressions. We observe that Weibull distributions result in slightly superior size correlation among similar sediment populations (see supporting information).

We then progress from this unconstrained "black-box" approach (Weltje & Prins 2007) by using the advantage that each sample is described by two size distributions; reflecting its fully-dispersed, particulate condition and minimally-dispersed, mixed aggregate-particle condition. This computation is initiated assuming a larger than expected number of evenly distributed hypothetical CPs in the fully-dispersed size distribution. Unlikely small and near-identical CPs that produce warning messages from the software are rejected. The means (modes) of the remaining CPs that describe the fully-dispersed size distribution best are then used to partially constrain the calculation of finer CPs in the minimally-dispersed size distribution, leaving additional CPs unconstrained. The rationale behind this approach is that the same elementary particle populations, or composites of them if aggregated, must be present in both distributions. Therefore, CPs comprising entirely of aggregates, in a minimally-dispersed size distribution simply register with a near-zero relative proportion. This approach has the additional important advantage that as the same CPs are quantified in both sample expressions, aggregation *per se* can be quantified.

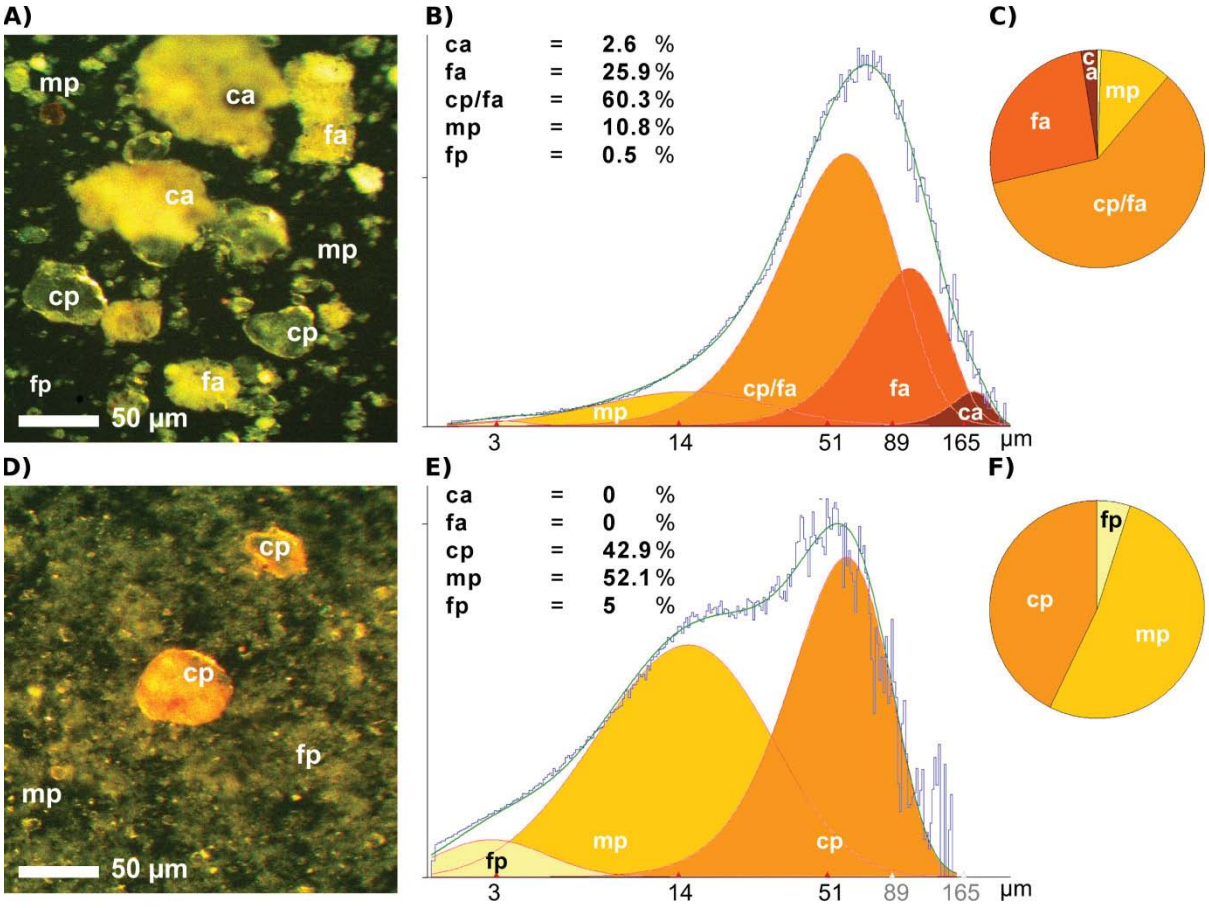

Fig. 1) *Comparison of minimally- and fully-dispersed expressions of sample 'BRA07-AR' 328 from the lowermost light band;* ***(A)*** *minimally-dispersed sample in microscopic view,* ***(B)*** *as decomposed sediment-size distribution,* ***(C)*** *as a pie-chart of relative proportions of its component populations (ca - coarse aggregates, fa - fine aggregates, cp - coarse particles, mp - moderate particles, fp - fine particles). Likewise, the depiction of the fully-dispersed sample expression* ***(D, E, F)****.*

Results

The postulated upward-fining successions between light and overlying dark bands were not detectable from conventional fully-dispersed particle-size analyses and total-sample statistics. The mean, median and modal size of the fully-dispersed light and dark bands are, within statistical error ranges, identical (Table 1A). In contrast, vertical size-trends from light to dark bands are readily apparent from Component Population Analysis. The initial unconstrained CPA assuming three CPs shows a clear upward-fining trend (Table 1B). A more detailed and genetically more meaningful picture of fining- upward trends emerges from the actual sediment populations in the partially-constrained CPA runs (Table 1C). The bands analysed in this manner consist of four to five discrete CPs. The results for a single exemplary sample from the lowermost light band are shown in Figure 1. The minimally-dispersed size distribution has two aggregate CPs; coarse aggregates (*ca*; ~165 µm)

and fine aggregates (*fa*; ~89 µm), (Fig. 1A and B), which disappear when fully dispersed (Fig. 1D and E). The three fine CPs are largely composed of particles; coarse particles (*cp*; ~51 µm), moderate particles (*mp*; ~14 µm) and fine particles (*fp*; ~3 µm). However, the ~51 µm CP comprises a mixture of similar-sized particles and aggregates reflected in the considerable overlap of the populations (*cp*) and (*fa*), (Fig. 1B) and as evident from microscopic observations (Fig. 1A and D).

A)	FD Mean (in µm)	FD Median (in µm)	FD Mode (in µm)	B)	unconst. CP modes MD (MDN in µm)	unconst. CP modes FD (MDN in µm)	C)	p. const. CP modes (MDN in µm)	rel. prop. MD (in %)	rel. prop. FD (in %)	Changes MD => FD (in %)
Light bands											
coarse aggregates	30	**21**	43		169	47		**166**	12	0	**- 12**
fine aggregates								**75**	44	0	**- 44**
coarse particles					67	11		**51**	35	32	**- 3**
moderate particles								**13**	9	58	**+ 49**
fine particles					17	3		**3**	1	10	**+ 9**
Dark bands											
aggregates	28	**21**	49		110	40		**60**	65	0	**- 65**
coarse particles					54	11		**47**	19	24	**+ 5**
moderate particles								**17**	15	63	**+ 48**
fine particles					14	3		**3**	1	13	**+ 12**

Table 1) *Summary statistics:* ***(A)*** *Average mean, median and mode of conventional fully-dispersed (FD) particle-size distributions for the samples of light and dark bands, respectively. The corresponding results of both* ***(B)*** *initial unconstrained (unconst.) and* ***(C)*** *final partially-constrained (p. constr.) Component Populations Analyses are presented as averaged modes of discrete component populations. The relative proportions in both minimally-dispersed (MD) and fully-dispersed sample conditions are given. Proportional decreases and increases that result from the breakdown of aggregates are quantified for all corresponding component populations.*

The CP characteristics of all samples are shown in Figure 2, by plotting the individual modes of all CPs against their relative proportions in each sample. The CPs are grouped into aggregate (circles) and particulate (squares) populations; with component populations of light bands (shades of orange) differentiated from dark bands (shades of blue). The breakup of the aggregate CPs is evident from their disappearance following dispersion with an equivalent proportional increase of particulate CPs in the fully-dispersed samples (triangles, with colours corresponding to light and dark bands).

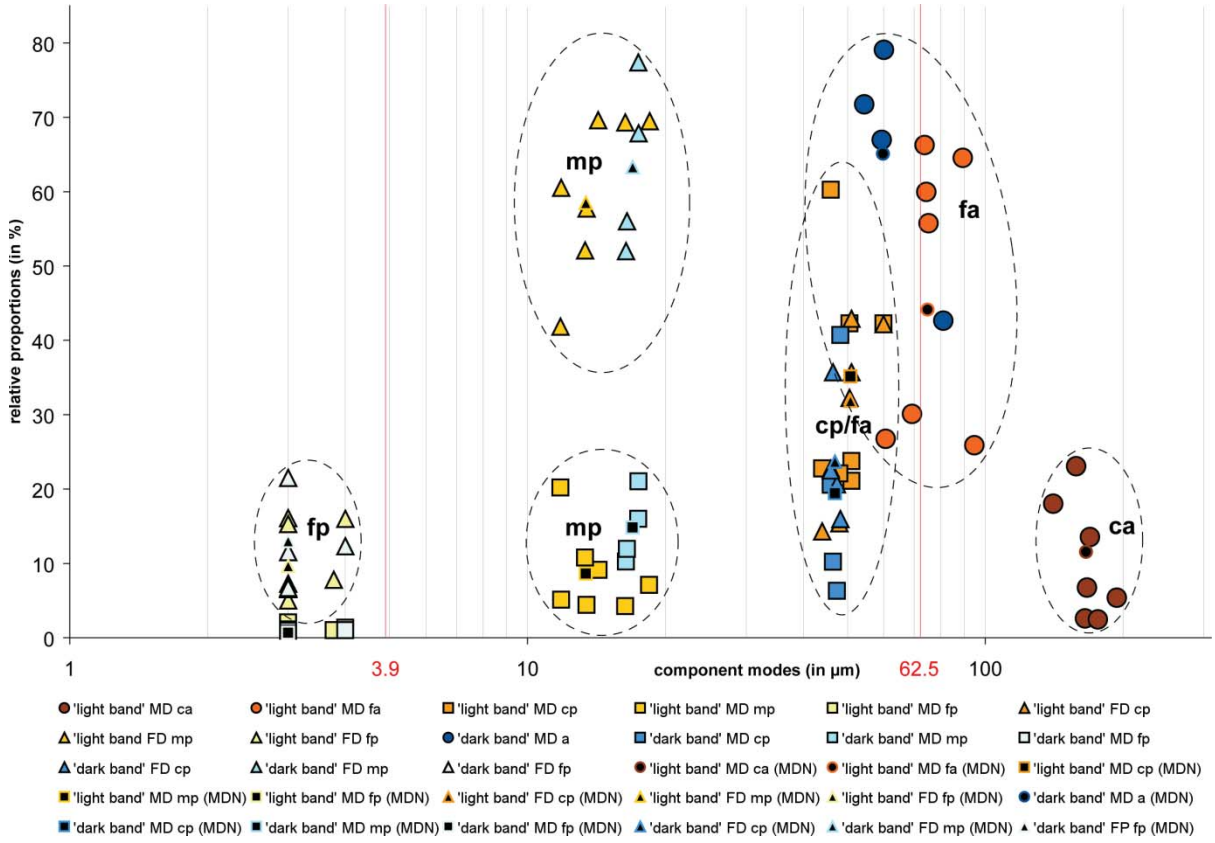

Fig. 2) *Cluster plot of all component population modes (on logarithmic scale) versus their corresponding relative proportions. Light and dark bands are colour-coded for both minimally-dispersed (MD) and fully-dispersed (FD) sample expressions. Medians (MDN) across component populations of related size classes are indicated.*

The percentage of aggregates within a sample can be calculated by taking the relative proportions of each CP containing aggregates in the minimally-dispersed size distribution (Fig. 1B) and subtracting their fully-dispersed equivalent CP (Fig. 1E). In the example, the fully-aggregated ~165 µm (*ca*) and ~89 µm (*fa*) CPs contribute ~28.5% to the total size distribution, and aggregates within the ~51 µm CP make up an additional ~17.4%. Table 1C shows that for all light band samples, the coarsest two CPs are entirely composed of aggregates and make up ~56% of the total size distribution. Overall, an average of only ~3% of the equivalent ~51 µm (*cp*) CP is aggregated. In contrast, the dark bands display only one aggregate (*a*) population making up 65% of the total size distribution. With an average mode of ~60 µm, it is slightly smaller than the finer aggregated population of the light bands. Its dispersion contributes to all three elementary particle populations which, within statistical error ranges, are identical to those of the underlying light bands. It should be noted that the finest clay-sized CP is close to the detection limit of the sizing technique used here, as indicated by the abrupt drop in the plotted curve (Fig. 1B and E). The actual mode and relative proportion of this CP will therefore differ slightly from the obtained results. Across all samples, the particles making up

the aggregates are largely silt-sized particles (~74-~84%), with clay-sized particles contributing the remainder (Table 1; Fig. 2).

Discussion

The results of this Component Population Analysis can be used to infer the depositional environment and provenance of the samples. While the total sample statistics from a conventional particle-size analysis (i.e. fully-dispersed) fail to register vertical size-trends between light and dark bands, the CPA performed on minimally- and fully-dispersed size distributions detects clear upward-fining trends. The detailed process interpretation is that with each successive flood flux, aggregates, as the coarsest constituents, settle out of suspension first. This is reflected in the two sand-sized aggregate CPs in the light bands, while the overlying dark bands feature only one finer silt-sized aggregate CP (*a*). The fluvial deposition process is therefore best reflected by the aggregates in both bands. In contrast, the particulate CPs do not reflect any vertical size trends between light and dark bands and have very similar size modes. This relative uniformity of the particle size within both the light and dark bands (Fig. 2) is in contrast to the local catchment lithology and supports the earlier inference of Williams and Nitschke (Williams & Nitschke 2005) that the fine-grained alluvial valley-fill deposits of the Flinders Ranges have an allochthonous aeolian origin (loess). The modal sizes of these particulate CPs compare well with those of fluvially-reworked loess in China (Sun et al. 2002), carried out fully-dispersed. Perhaps most significantly, the present field study supports the evidence from the laboratory experiments of Schieber and colleagues (Schieber et al. 2007) that transport-stable mud aggregates are formed by flocculation in turbulent waters, and applies it to terrestrial fluvial environments.

Conclusions

The sediment sizing protocol outlined here represents a breakthrough in the size analysis of alluvial sediments. It is now possible to establish the provenance and geomorphic processes operating in the formation of partially-aggregated sediments in a range of environments; from late Pleistocene fine-grained valley-fills (K. Heine & J. T. Heine 2002) in particular, to the mudstones in the geological record in general (Macquaker & Bohacs 2007)(Wright & Marriot 2007). The method also resolves numerical instabilities inherent in the parametric decomposition of single unimodal size distributions (Weltje & Prins 2007), by correlating size distributions of different dispersion states of each sample. The very nature of aggregation can now be examined with a freely-available quantitative tool, capable of resolving discrete aggregate and elementary particle populations. This new methodology

has the potential to open the door to a wide range of studies, striving to relate sediment size signatures to sources and formative processes within the landscape.

Acknowledgements

We thank CRC LEME (Cooperative Research Centre for Landscape Environments and Mineral Exploration), the Australian Research Council (ARC grant #DP0559577) and the ARC Environmental Futures Network (grant #58103136) for generous financial support. Thanks also to the Flinders Ranges National Park authorities for research permits and friendly accommodation, Craig Strong for introduction and assistance in the laboratory, and Peter D. M. MacDonald for inspiring correspondence concerning the “Mixdist” software package.

References

van Andel, T.H. (1973) Texture and dispersal of sediments in the Panama Basin. *J. Geol.*, **81**, 434-457.

Bagnold, R.A. (1937) The size-grading of sand by wind. *Proceedings of the Royal Society of London*, **A 163**, 252-264.

Bagnold, R.A. (1941) *The physics of blown sand and desert dunes*, London, Methuen & Co. Ltd, pp. 265.

Bagnold, R.A. and **Barndorff-Nielsen, O.** (1980) The pattern of natural size distributions. *Sedimentology*, **27**, 199-207.

Beattie, J.A. (1970). Peculiar features of soil development in parna deposits in the eastern Riverina, N.S.W. *Aust. J. Soil Res.*, **8**, 145-156.

Beckman Coulter (2002) *Multisizer 3 Operator's Manual PN8321681*. Fullerton, California, Beckman Coulter, Inc.

Butler, B.E. (1955). A system for the description of soil structure and consistence in the field. *J. Aust. Inst. of Agricultural Science*, **1**, 231-252.

Butler, B.E. (1976). Subplasticity in Australian Soils. Introduction. *Aust. J. Soil Res.*, **14**, 225-226.

Clark, M.W. (1976) Some methods for statistical analysis of multimodal distributions and their application to grain-size data. *Math. Geol.*, **8(3)**, 267-282.

Crocker, R.L. (1946) The Simpson Desert Expedition, 1939 Scientific Reports: No. 8 - The soils and vegetation of the Simpson Desert and its borders. *Trans. Roy. Soc. S. Aust.*, **70(2)**, 235-264.

Dare-Edwards, A.J. (1982). Clay pellets of clay dunes: types, mineralogy, origin and effect of pedogenesis. In: *Quaternary dust mantles of China, New Zealand and Australia* (Ed.) R.J. Wasson, Canberra: Australian National University, pp. 179-189.

Dauphin, J.P. (1980) Size distribution of chemically extracted quartz used to characterize fine-grained sediments. *J. Sed. Petrol.*, **50(1)**, 205-214.

Doeglas, D.J. (1946) Interpretation of the results of mechanical analyses. *J. Sed. Petrol.*, **16(1)**, 19-40.

Folk, R.L. (1971) Longitudinal dunes of the northwestern edge of the Simpson Desert, Northern Territory, Australia. 1. Geomorphology and grain size relationships. *Sedimentology*, **16**, 5-54.

Folk, R.L. and **Ward, W.C.** (1957) Brazos River bar: a study in the significance of grain size parameters. *J. Sed. Petrol.*, **27(1)**, 3-26.

Fuller, A.O. (1962) Systematic fractionation of sand in the shallow marine and beach environment off the South African Coast. *J. Sed. Petrol.*, **32(3)**, 602-606.

Goossens, D. (2008) Techniques to measure grain-size distributions of loamy sediments: a comparative study of ten instruments for wet analysis. *Sedimentology*, **55**, 65-96.

Harris, S.A. (1958) Probability curves and the recognition of adjustment to depositional environment. *J. Sed. Petrol.*, **28(2)**, 151-163.

Heine, K. and **Heine, J.T.** (2002) A paleohydrologic reinterpretation of the Homeb Silts, Kuiseb River, central Namib Desert (Namibia) and paleoclimatic implications. *Catena*, **48**, 107-130.

Ibbeken, H. (1983) Jointed source rock and fluvial gravels controlled by Rosin's law: a grain-size study in Calabria, South Italy. *J. Sed. Res.*, **53(4)**, 1213-1231.

Inman, D.L. (1952) Measures of describing the size distribution of sediments. *J. Sed. Petrol.*, **22(3)**, 125-145.

Kochel, R.C. and **Baker, V.R.** (1982) Paleoflood analysis. *Science*, **215**, 353-361.

Kochel, R.C. and **Baker, V.R.** (1988) Paleoflood analysis using slackwater deposits. In: *Flood Geomorphology* (Eds. V.R. Baker and R.C. Kochel), New York: John Wiley & Sons, pp. 357-376.

Kondolf, G.M. and **Adhikari, A.** (2000) Weibull vs. lognormal distributions for fluvial gravels. *J. Sed. Petrol.*, **70(3)**, 456-460.

Krumbein, W.C. and **Tisdel, F.W.** (1940) Size distributions of source rocks of sediments. *Am. J. Sci.*, **238**, 296-305.

Leys, J., McTainsh, G.H., Koen, T., Mooney, B. and **Strong, C.** (2005) Testing a statistical curve-fitting procedure for quantifying sediment populations within multi-modal particle-size distributions. *Earth Surf. Proc. Land.*, **30**, 579-590.

Macdonald, P.D.M. and **Green, P.E.J.** (1988) *User's guide to program MIX: an interactive program for fitting mixtures of distributions*, Ontario, Canada: Ichthus Data Systems.

Macdonald, P.D.M. and **Du, J.** (2004) *Mixdist: Mixture Distribution Models. R package version 0.5-2*. http://cran.r-project.org/web/packages/mixdist/index.html [Accessed September 29, 2008].

Macquaker, J.H.S. and **Bohacs, K.M.** (2007) On the accumulation of mud. *Science*, **318**, 1734-1735.

McCammon, R.B. (1962) Moment measures and the shape of size frequency distributions. *J. Geol.*, **70**, 89-92.

McIntyre, D.S. (1976). Subplasticity in Australian soils. 1 description, occurrence, and some properties. *Aust. J. Soil Res.*, **14**, 227-236.

McTainsh, G.H., Lynch, A.W. and **Hales, R.** (1997) Particle-size analysis of aeolian dusts, soils and sediments in very small quantities using a Coulter Multisizer. *Earth Surf. Proc. Land.*, **22**, 1207-1216.

Oser, R.K. (1972) Sedimentary components of northwest Pacific pelagic sediments. *J. Sed. Petrol.*, **42(2)**, 461-467.

Otto, G.H. (1939) A modified logarithmic probability graph for the interpretation of mechanical analyses of sediments. *J. Sed. Petrol.*, **9(2)**, 62-76.

R Development Core Team (2008) R: a language and environment for statistical computing. In: R Foundation for Statistical Computing, Vienna, Austria, http://www.r-project.org/.

Richardson, H. (1903) Sea sand. A lecture before the Yorkshire Philosophical Society, Dec. 1902. *Annual Report of the Yorkshire Philosophical Society*, **1902**, 43-58.

Rust, B.R. and **Nanson, G.C.** (1989). Bedload transport of mud as pedogenic aggregates in modern and ancient rivers. *Sedimentology*, **36**, 291-306.

Schieber, J., Southard, J. and **Thaisen, K.** 2007. Accretion of mudstone beds from migrating floccule ripples. *Science*, **318**, 1760-1763.

Sheridan, M.F., Wohletz, K.H. and **Dehn, J.** (1987) Discrimination of grain-size subpopulations in pyroclastic deposits. *Geology*, **15(4)**, 367-370.

Sindowski, K.H. (1957) Die synoptische Methode des Kornkurven-Vergleichs zur Ausdeutung fossiler Sedimentionsräume. *Geol. Jb.*, **73**, 235-275.

Spencer, D.W. (1963) The interpretation of grain size distribution curves of clastic sediments. *J. Sed. Petrol.*, **33(1)**, 180-190.

Sun, D., Rea, D.K., Vandenberghe, J., Jiang, F., An, Z. and **Su, R.** (2002) Grain-size distribution function of polymodal sediments in hydraulic and aeolian environments, and numerical partitioning of the sedimentary components. *Sed. Geol.*, **152**, 263-277.

Tanner, W.F. (1958) The zig-zag nature of Type I and Type IV curves. *J. Sed. Petrol.*, **28(3)**, 372-375.

Udden, J.A. (1898) The mechanical composition of wind deposits. *Augustina Library Publ.*, **1**, 1-69.

Udden, J.A. (1914) Mechanical composition of clastic sediments. *Geol. Soc. Am. Bull.*, **25**, 655-744.

Visher, G.S. (1969) Grain size distributions and depositional processes. *J. Sed. Petrol.*, **39(3)**, 1074-1106.

Walger, E. (1962) Die Korngrössenverteilung von Einzellagen sandiger Sedimente und ihre genetische Bedeutung. *Geol. Rundsch.*, **51(2)**, 494-507.

Weltje, G.J. and **Prins, M.A.** (2007) Genetically meaningful decomposition of grain-size distributions. *Sed. Geol.*, **202**, 409-424.

Wentworth, C.K. (1922) The shape of beach pebbles. *US Geol. Surv. Prof. Pap.*, **131(C)**, 75-83.

Williams, M.A.J. and **Nitschke, N.** (2005) Influence of wind-blown dust on landscape evolution in the Flinders Ranges, South Australia. *S. Aust. Geogr. J.*, **104**, 25-36.

Wright, P. and **Marriot, S.B.** (2007) The dangers of taking mud for granted: lessons from Lower Old Red Sandstone dryland river systems of South Wales. *Sed. Geol.*, **195**, 91-100.